

1 **Underappreciated contributions of biogenic volatile organic compounds from urban**
2 **greening spaces to ozone pollution: a high-resolution modeling study**

3
4 Haofan Wang^{1,2,3,4}, Yuejin Li^{1,2,3}, Yiming Liu^{1,2,3*}, Xiao Lu^{1,2,3}, Yang Zhang⁵, Qi Fan^{1,2,3*}, Chong Shen⁶,
5 Senchao Lai⁷, Yan Zhou⁸, Tao Zhang⁸, Dingli Yue⁸

6
7 ¹*School of Atmospheric Sciences, Sun Yat-sen University, and Southern Marine Science and Engineering Guangdong Laboratory*
8 *(Zhuhai), Zhuhai, 519082, P. R. China*

9 ²*Guangdong Provincial Field Observation and Research Station for Climate Environment and Air Quality Change in the Pearl*
10 *River Estuary, Guangzhou, 510275, P. R. China*

11 ³*Guangdong Province Key Laboratory for Climate Change and Natural Disaster Studies, Sun Yat-sen University, P. R. China*

12 ⁴*Centre for Atmospheric Science, Department of Earth and Environmental Sciences, The University of Manchester, Manchester,*
13 *United Kingdom*

14 ⁵*College of Resources and Environment, Chengdu University of Information Technology, Chengdu, Sichuan, China*

15 ⁶*Guangzhou Climate and Agrometeorology Center, Guangzhou 511430, China*

16 ⁷*The Key Lab of Pollution Control and Ecosystem Restoration in Industry Clusters, Ministry of Education, School of Environment*
17 *and Energy, South China University of Technology, Guangzhou 510006, China*

18 ⁸*National Key Laboratory for Regional Air Quality Monitoring of Environmental Protection/Guangdong Ecological Environment*
19 *Monitoring Center, Guangzhou 510308, P. R. China*

20
21 *Correspondence to:* Yiming Liu (liuym88@mail.sysu.edu.cn), Qi Fan (cesfq@mail.sysu.edu.cn)
22

Abstract

Urban Green Spaces (UGS), such as parks, and gardens, are widely promoted as a strategy for improving the urban ~~atmosphere and environmental health~~atmospheric environment. However, this study reveals that it can exacerbate urban ozone (O₃) levels under certain conditions, as demonstrated by a September 2017 study in Guangzhou, China. ~~Utilizing~~Using the Weather Research and Forecasting Model with the Model of Emissions of Gases and Aerosols from Nature (WRF-MEGAN) and the Community Multiscale Air Quality (CMAQ) model ~~with a high horizontal resolution (1 km)~~, we assessed the impact of UGS-related biogenic volatile organic compound (BVOC) emissions on urban O₃. Our findings indicate that the UGS-BVOC emissions in Guangzhou amounted to 666 Gg (~90 Mg/km²), with isoprene (ISOP) and monoterpene (TERP) contributing remarkably to the total UGS-BVOC emissions. Compared to anthropogenic VOC (AVOC) and BVOC emissions, UGS-BVOC emissions account for ~33.45% in the city center, and their inclusion in the model reduces ISOP underestimation. ~~In comparison to anthropogenic VOC (AVOC) and BVOC emissions, UGS-BVOC emissions account for approximately 33.45% in the city center region. Incorporating UGS-BVOC emissions into the model significantly reduces the underestimation of ISOP levels compared to observations.~~ The study shows ~~improvements in~~improved simulation mean biases for MDA8 O₃, from -3.63 to -0.75 ppb in the city center ~~region~~. Integrating UGS-BVOC and UGS-LUCC (Land Use Cover Change) enhances surface monthly mean O₃ by 1.7–3.7 ppb (+3.8–8.5%) and adds up to 8.9 ppb (+10.0%) to MDA8 O₃ during pollution episodes. ~~UGS-BVOC and UGS-LUCC (land use cover changes) integration in the air quality model notably enhances surface monthly mean O₃ predictions by 1.7–3.7 ppb (+3.8–8.5%) and contributes up to 8.9 ppb (+10.0%) to MDA8 O₃ during O₃ pollution episodes.~~ UGS-BVOC emissions alone increase monthly mean O₃ by 1.0–1.4 ppb (+2.3–3.2%) in urban areas and contribute up to 2.9 ppb (+3.3%) to MDA8 O₃ during pollution episodes. ~~Additionally, UGS-BVOC emissions alone increase the monthly mean O₃ levels by 1.0–1.4 ppb (+2.3–3.2%) in urban areas and contribute up to 2.9 ppb (+3.3%) to MDA8 O₃ levels during O₃ pollution episodes.~~ These impacts can extend to surrounding suburban and rural areas through regional transport, highlighting the ~~importance of accurately accounting for UGS-BVOC emissions to better understand and manage their impact on regional air quality.~~ need to accurately account for UGS-BVOC emissions to better manage air quality.

51 **Keywords**

52 Urban green space; BVOC; Ozone; Land use cover; CMAQ; MEGAN
53

54 **1. Introduction**

55 Exposure to air pollution now accounts for more fatalities than malaria, tuberculosis, and HIV/AIDS combined
56 (Lelieveld et al., 2020). As a result, the World Health Organization has declared air pollution the most
57 significant environmental threat to human health (WHO, 2021). Notably, over 70% global health burden of
58 air pollution stems from human-made emissions, leading to a policy focus predominantly on reducing these
59 emissions (Chowdhury et al., 2022; Lelieveld et al., 2019). Despite proactive measures to curb anthropogenic
60 emissions, the incidence of ozone episodes is escalating alongside rapid urbanization (Lu et al., 2020; Yim et
61 al., 2019). Numerous studies have investigated the effects of land use cover changes (LUCC) on air quality
62 during urbanization using numerical models and the majority of these studies conclude that urbanization
63 exacerbates air pollution (Qiu et al., 2023; Wang et al., 2022). However, such studies that depend on numerical
64 models usually face the coarse-resolution land use cover data limitation (Ma et al., 2022, 2019), which leads
65 these studies to frequently overlook a passive abatement approach distinct from reducing anthropogenic
66 sources—namely, the cultivation of urban green spaces (UGS) (Cohen et al., 2017).

67
68 The widely accepted notion that UGS can enhance air quality is substantiated by various strands of literature,
69 including public health (Burnett et al., 2018), urban planning (Solomon, 2007), and ecosystem services
70 (Lohmann et al., 2010). This concept is not only prevalent in scholarly circles but also gains traction in popular
71 media and is echoed in international standards and policy frameworks. For instance, the United Nations
72 System of Environmental-Economic Accounting advocates for vegetation as a nature-based approach to
73 mitigate air pollution (Le Page et al., 2015). Vegetation primarily contributes to air pollution reduction through
74 two mechanisms: deposition and dispersion (Shindell et al., 2012). Deposition involves the absorption of air
75 pollutants onto vegetative surfaces, while dispersion refers to the reduction of air pollutant concentrations
76 through aerodynamic effects caused by vegetation (Tiwari and Kumar, 2020; N. Wang et al., 2019a). Notably,
77 Ramanathan et al. (2001) reported that dispersion effects are significantly more impactful than deposition,
78 exceeding it by an order of magnitude via a radiative forcing modeling method.

80 However, the efficacy of dispersion effects resulting from UGS-LUCC in reducing air pollution is not
81 straightforward. These effects can, under certain conditions, even increase local air pollution concentrations.
82 These conditions are influenced by several factors, such as the specific structure of the UGS vegetation
83 properties (e.g., height, leaf density), the site context (e.g., street canyon geometry, proximity to emission
84 sources), and prevailing meteorological conditions (e.g., wind speed and direction) (Jin et al., 2017; Tomson
85 et al., 2021; Yang et al., 2020). For example, dense tree canopies might impede ventilation in urban street
86 canyons, while porous vegetation barriers in open-road settings could potentially intensify roadside air
87 pollution concentrations (Chen et al., 2021; Jin et al., 2014). Furthermore, Seinfeld et al., (1998) underscores
88 the complexity of these interactions, and demonstrated that vegetation could exert nonlinear effects on
89 meteorological processes. These effects are particularly evident in their impact on the Planetary Boundary
90 Layer Height (PBLH) and the turbulent transport and advection of pollutants, which in turn influence
91 dispersion conditions.

92
93 UGS also have a complex role in air quality due to their production of biogenic volatile organic compounds
94 (BVOCs). For instance, in cities like Los Angeles, the UGS-BVOC emissions contribute to a quarter of the
95 secondary organic aerosol formation on hot days (Schlaerth et al., 2023). While Guenther et al., (2012) noted
96 that the majority of BVOC emissions are from natural land cover, Ma et al., (2022) indicates that in
97 metropolitan areas, the UGS-BVOC emissions can be significantly higher, ranging from 1 to 30 times those
98 from natural land use cover. This evidence suggests a dual nature of UGS vegetation in urban environments:
99 it can mitigate air pollution under certain conditions, but conversely, there is substantial experimental and
100 modeling evidence showing it can exacerbate pollution under different circumstances (Allen and Ingram, 2002;
101 Burnett et al., 2018; Cohen et al., 2017). Moreover, metropolitan areas often encounter VOC-limited
102 conditions, or NO_x -saturation, where even minimal BVOC emissions can lead to notable O_3 production (P.
103 Wang et al., 2019). Additionally, urban areas typically experience higher temperatures than their surrounding
104 natural landscapes due to the urban heat island effect (Masson-Delmotte et al., 2021). This increase in
105 temperature is likely to further amplify the UGS-BVOC emissions (Zhou et al., 2015), influencing O_3
106 concentrations significantly. This interaction might explain why many regional numerical models
107 underestimate urban surface ozone levels, as they often lack high-resolution land use cover data necessary to
108 accurately estimate the UGS-BVOC emissions (Qiu et al., 2023; Wang et al., 2021; Wu et al., 2020).

110 Currently, there is a growing research interest in characterizing the air quality impacts of UGS. While
111 Arghavani et al., (2019) investigated the effects of UGS on gaseous air pollutants in Tehran using the WRF-
112 Chem model, their focus was on the impact of meteorological changes on O₃ resulting from UGS (i.e., UGS-
113 LUCC effects), rather than the UGS-BVOC emissions effects on O₃. In contrast, Schlaerth et al., (2023a)
114 addressed the influence of the UGS-BVOC emissions on O₃ in Los Angeles and their findings indicate that
115 the UGS-BVOC emissions may increase O₃ by 0.95 ppb during the daytime and decrease it by 0.41 ppb at
116 night. Despite Schlaerth et al., (2023a) illustrating the significance of the UGS-BVOC emissions on O₃
117 concentrations, they did not investigate the impact of the UGS-LUCC effects.

118
119 Surface O₃ is generally formed through chemical reactions of VOCs and NO_x in the presence of sunlight. The
120 nonlinear correlation between O₃ and concentrations of BVOC and NO_x underscores the importance of
121 examining potential interactions between the UGS-BVOC emissions and anthropogenic emissions.
122 Furthermore, recent studies have highlighted the significance of the UGS-LUCC effects and the UGS-BVOC
123 emissions effects. Given the rise in urban O₃ pollution, investigating the influence of the UGS-LUCC effects
124 and the UGS-BVOC emissions effects on O₃ can assist in rationalizing UGS planning and formulating air
125 quality mitigation strategies. However, there is a lack of quantification regarding the combined effects of
126 UGS-LUCC and UGS-BVOC emissions on O₃.

127
128 Situated in South China, Guangzhou ([Figure 1](#)~~Figure 1~~) is one of the rapidly expanding cities in China since
129 the initiation of the reform and opening-up policy, undergoing swift urbanization (Yao and Huang, 2023).
130 Being a key city in the Guangdong-Hongkong-Macao Greater Bay Area, Guangzhou places significant
131 emphasis on UGS development. In this study, we aim to reconstruct the leaf area index (LAI) dataset for urban
132 areas and estimate the UGS-BVOC emissions utilizing the Model of Emissions of Gases and Aerosols from
133 Nature version 3.1 (MEGANv3.1) (Guenther et al., 2020a). Subsequently, employing the Weather Research
134 and Forecast model version 4.1.1 (WRFv4.1.1) (Salamanca et al., 2011) – Community Multiscale Air Quality
135 model version 5.4 (CMAQv5.4) (<https://zenodo.org/record/7218076>, last accessed: June 3, 2023), we intend
136 to estimate the improvements of the CMAQ simulation performance from considering UGS-LUCC and UGS-
137 BVOC and investigate the UGS-LUCC effects, the UGS-BVOC emissions effects, and their combined
138 impacts on O₃ over Guangzhou by configuring sensitivity cases.

2. Methods and data

2.1 Leaf area index and land cover dataset

The default LAI dataset to drive the MEGANv2.1 model which can be used for MEGANv3.1 is derived from the enhanced Moderate Resolution Imaging Spectroradiometer (MODIS)/MOD15A2H in 2003 with 1 km spatial resolution (Myneni et al., 2015). As MODIS/MOD15A2H assigns an LAI value of 0 to urban areas, MEGANv3.1 compensates by averaging the LAI values in the vicinity of the urban area. However, this approach introduces considerable uncertainty in the estimation of UGS-BVOC emissions. Hence, we opted for the Global Land Surface Satellite (GLASS) LAI product for MEGANv3.1 in 2017 with 500-m spatial resolutions, derived from MODIS surface reflectance data using the bidirectional long short-term memory (Bi-LSTM) model, which leverages existing global LAI products (Ma and Liang, 2022) and effectively incorporates the temporal and spectral information of MODIS surface reflectance. Consequently, the valid values of this data extend to urban areas, making it suitable for simulating the UGS-BVOC emissions.

In this study, UGS are delineated as vegetation areas within the urban grid, and the urban grids are derived from MODIS/MCD12Q1 (Friedl and Sulla-Menashe, 2019) in 2017, which corresponds to the simulation period with 500 m spatial resolution. Furthermore, a high-resolution (10 m) land cover dataset in 2017 was also obtained from the Geographic Remote Sensing Ecological Network Platform (accessible at <http://www.gisrs.cn/infofordata?id=1c089287-909e-4394-b07f-c7004be60884>, last accessed: 20/11/2023) and was employed to depict the spatial patterns of UGS. The processed land cover dataset is illustrated in Figure S1. Meanwhile, the use of high-resolution land use cover data is pivotal for accurately depicting the intricate details of land use cover, especially in areas broadly classified as urban by coarse-resolution data (i.e., MCD12Q1) and this refined approach allows for a more precise differentiation of UGS. Specifically, we maintain a consistent urban area definition across both land use cover datasets, anchored by the urban delineation provided by the MCD12Q1 dataset. However, the coarse resolution of MCD12Q1 is insufficient for detailed spatial characterization of UGS. To address this limitation, we employ the high-resolution dataset to refine the characterization of non-urban surfaces within the urban boundaries (i.e., UGS) defined by MCD12Q1. This approach yields a sophisticated land cover dataset with 10 m spatial resolution that retains the urban extent delineated by MCD12Q1 while incorporating detailed representations of UGS absent in the original dataset. Consequently, while both datasets encompass identical urban extents, the default dataset lacks

168 representations of UGS, in contrast to the high-resolution dataset, which includes detailed depictions of UGS.

169 2.2 MEGANv3.1 configuration

170 The calculation of BVOC emissions was performed utilizing MEGANv3.1 (accessible at
171 <https://bai.ess.uci.edu/megan>, last accessed: 21 November 2023), which is a newly updated version.
172 MEGANv3.1 estimates BVOC emissions as the product of an emission factor and an emission activity factor
173 (Guenther et al., 2020a):

$$174 E = EF \times \gamma \quad (\text{Eq. 1})$$

175
176 In this equation, E is the net emission flux ($\mu\text{g m}^{-2} \text{h}^{-1}$), and EF is the weighted average of the emission
177 factor ($\mu\text{g m}^{-2} \text{h}^{-1}$) for each vegetation type calculated by Emission Factor Processor (EFP). The emission
178 activity factor (γ) considers emission responses to changes in environmental and phenological conditions.
179 Compare with earlier versions, γ in MEGANv3.1 adds quantifications for responses to high and low
180 temperature, high wind speed, and air pollution (O_3).

$$181 \gamma = LAI \times \gamma_{TP} \times \gamma_{LA} \times \gamma_{SM} \times \gamma_{HT} \times \gamma_{LT} \times \gamma_{HW} \times \gamma_{CO_2} \times \gamma_{BD} \times \gamma_{O_3} \quad (\text{Eq. 2})$$

182
183 In this equation, the activity factor denotes the emission response to canopy temperature/light (γ_{TP}), leaf age
184 (γ_{LA}), soil moisture (γ_{SM}), high temperature (γ_{HT}), low temperature (γ_{LT}), high wind speed (γ_{HW}), ambient
185 CO_2 concentration (γ_{CO_2}), bidirectional exchange (γ_{BD}), O_3 exposure (γ_{O_3}), and Leaf Area Index (LAI). In
186 this study, γ_{CO_2} was not considered in the BVOC emission estimation. It is worth noting that MEGANv3.1
187 uses the 2-m temperature variable from the WRF model to calculate BVOC emissions. ~~Meanwhile, The~~
188 ~~MEGANv3.1 approach can calculate the emissions at each canopy level as the product of the emission~~
189 ~~factor and emission activity at each level.~~

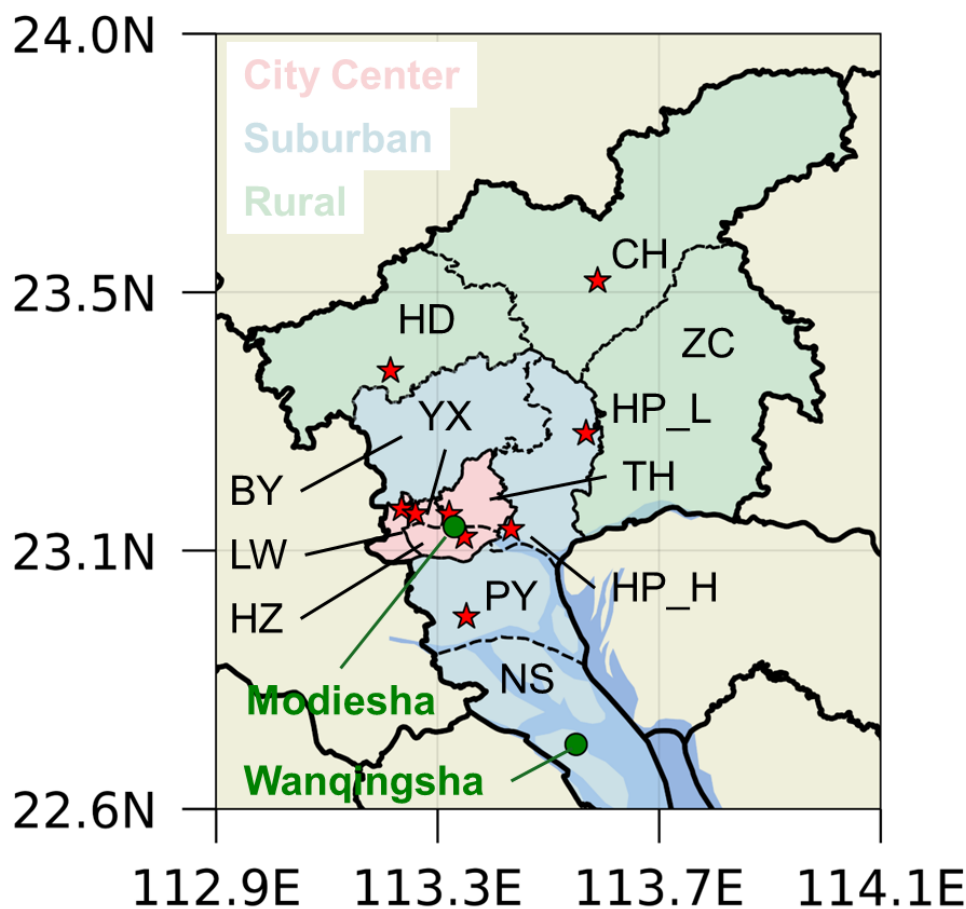
190
191 Hence, the input data to drive MEGANv3.1 comprises meteorological variables (e.g., temperature, solar
192 radiation, relative humidity, soil moisture), LAI, and three types of land cover data (i.e., ecotype, growth
193 form, and relative vegetation composition for each ecotype/growth form). ~~Meanwhile, the~~ growth form
194 datasets in MEGANv3.1 contain considerations of evergreen broadleaf forests, grasslands, and crops, which
195 cover all types of UGS in Guangzhou city (Figure S1). Meteorological data are obtained from the WRF

196 simulation results, and the LAI dataset is detailed in Section 2.1 as well as additional default land cover data
197 provided by MEGANv3.1 were employed.

198 **2.3 WRF-CMAQ and Case Configuration**

199 Both the WRFv4.1.1 model and the CMAQv5.4 model are compiled and operated on a server with a Linux
200 environment. The WRFv4.1.1 model was employed to simulate meteorological conditions, utilizing initial and
201 boundary conditions sourced from the NCEP $1^\circ \times 1^\circ$ Final (FNL) reanalysis dataset (National Centers for
202 Environmental Prediction, National Weather Service, NOAA, U.S. Department of Commerce, 2000). As
203 illustrated in Figure S2, four nested domains with horizontal resolutions of 27, 9, 3, and 1 km, respectively,
204 were employed. The outermost domain encompasses mainland China, while the innermost domain zooms in
205 Guangzhou city, and the physical parameterization configured for the WRF simulation is listed in Table S1.
206 CMAQv5.4 utilized meteorological fields provided by WRF to model O_3 concentrations. The initial and
207 boundary conditions for the CMAQ model were derived from the default profiles representing a clean
208 atmosphere. In addition, we acquired anthropogenic emissions for the CMAQ domain from the Multi-
209 resolution Emission Inventory for China (MEIC) 2017 developed by Tsinghua University, which contains
210 monthly gridded ($0.25^\circ \times 0.25^\circ$) emissions information for anthropogenic emissions. Moreover, the CMAQ
211 model was configured with the Carbon Bond chemical mechanism (CB06) (Luecken et al., 2019) and AERO7
212 (Pye et al., 2017). In this study, we incorporated the Modular Emission Inventory Allocation Tools for the
213 Community Multiscale Air Quality model (MEIAT-CMAQ, <https://github.com/Airwhf/MEIAT-CMAQ>, last
214 accessed: February 27, 2024) to allocate spatial and species-specific emissions within the raw inventories,
215 addressing discrepancies in resolution and species compared to the modeled configurations. Moreover,
216 MEIAT-CMAQ can directly generate the hourly model-ready emission files for CMAQ via temporal
217 allocation. The model simulation spanned a month, from 21 August 2017 to 30 September 2017. To mitigate
218 bias resulting from meteorological and chemical drift, the initial 10 days of this simulation were designated
219 as spin-up and were not included in the analysis for this study. Given the spatial heterogeneity in the
220 distribution of UGS across different areas, this study categorizes Guangzhou into city center, suburban, and
221 rural regions (Figure 1). Specifically, the city center areas comprise Haizhu (HZ), Liwan (LW), Yuexiu
222 (YX), and Tianhe (TH) districts. The city center region has more UGS areas due to the higher urban land use
223 and land cover fraction (Figure S1) compared to the suburban and rural regions. The suburban areas
224 encompass Huangpu (HP), Baiyun (BY), Panyu (PY), and Nansha (NS) districts. Lastly, the rural regions

225 include Zengcheng (ZC), Conghua (CH), and Huadu (HD) districts. To facilitate clear differentiation between
226 the two sites in the HP region, they have been designated as HP_L and HP_H, respectively.



227
228 **Figure 1** The innermost domain of WRF-CMAQ with various areas and the air quality station locations map. Modiesha and Wanqingsha
229 are the observation sites for isoprene.

230
231 In this study, four distinct cases, as listed in [Table 1](#) were established to investigate the impacts of
232 UGS-LUCC, UGS-BVOC, and their combined effects on the ozone simulation. These cases also focused on
233 the performance of the CMAQ simulation and the influence on O₃ episodes. The Gdef_N case considered as
234 the base case, employs default land use cover data—specifically, data excluding UGS, and uses the LAI dataset
235 with urban areas omitted (N-LAI). In contrast, the Gdef_Y case is similar to Gdef_N but incorporates the LAI
236 dataset that includes urban areas (T-LAI). This adjustment allows for the assessment of the UGS-BVOC
237 emission effects on O₃ concentrations. The Ghr_N case mirrors Gdef_N but differs by integrating high-
238 resolution land use cover data, which encompasses UGS land use cover. This case aims to examine the UGS-
239 LUCC effects on O₃ concentrations. Finally, the Ghr_Y case combines high-resolution land use cover data
240 with the LAI dataset inclusive of urban areas, thereby enabling an exploration of the combined effects of UGS-
241 BVOC emissions and UGS-LUCC on O₃ concentrations.

Table 1 Case configurations. The default land cover (LC) datasets are derived from MODIS/MCD12Q1, while the high-resolution LC datasets use MODIS/MCD12Q1 for natural areas and the 10-m datasets from Geographic Remote Sensing Ecological Network Platform for urban areas. N-LAI (None-urban Leaf Area Index) indicates that the model uses LAI data without urban LAI, whereas T-LAI (Total LAI) includes urban LAI. The "Description" column explains the purpose of each case.

Name	LC dataset	LAI dataset	Description
Gdef_N	Default data	N-LAI	Base
Gdef_Y	Default data	T-LAI	UGS-BVOC effects
Ghr_N	High-resolution data	N-LAI	UGS-LUCC effects
Ghr_Y	High-resolution data	T-LAI	combined effects

2.4 Observation Dataset

We use the hourly ground-level meteorological observations, encompassing 2-m temperature (T2) and 10-m wind speed (WS10), sourced from national basic meteorological stations provided by the Guangdong Provincial Meteorological Service (Figure S3). Hourly ambient concentrations of O₃, CO, and NO₂ from national monitoring stations are gathered from the China National Environmental Monitoring Centre (CNEMC; <http://www.cnemc.cn>, last assess: 24 December 4, 2024). The real-time hourly concentration of O₃ was measured by the ultraviolet absorption spectrometry method and differential optical absorption spectroscopy at each monitoring site. NO₂ concentrations are measured by the molybdenum converter method known to have positive interferences from NO₂ oxidation products (Dunlea et al., 2007). The instrumental operation, maintenance, data assurance, and quality control were properly conducted based on the most recent revisions of China Environmental Protection Standards (Zhang and Cao, 2015), and the locations of these air quality stations are depicted in [Figure 1](#). Additionally, meteorological data also undergo thorough quality control. Subsequently, they are utilized to assess the model performance of WRF-CMAQ.

For the isoprene (ISOP) evaluation, we use observation data from the Modiesha (23.11°N, 113.33°E) and Wanqingsha (22.71°N, 113.55°E) sites ([Figure 1](#)), where an online gas chromatography-mass spectrometry/flame ionization detector system (GC-FID/MSD, TH 300B, Wuhan) is used to measure VOCs in the ambient atmosphere. The system has a sampling rate of 60 mL/min for 5 minutes per sample, with a sampling frequency of once per hour (Meng et al., 2022). The ISOP observation data undergo rigorous quality control, which can be used for evaluating simulated ISOP concentrations. It is worth noting that the ISOP

269 observational data for the Modiesha site covers September 2017, while the Wanqingsha site has data coverage
270 from September 7 to September 30, 2017.

271 **3. Results and discussion**

272 **3.1 Model Evaluation**

273 Evaluation of the WRF-CMAQ model performance is undertaken through comparison against ground-level
274 observations and the evaluation metrics of meteorological parameters are listed in Table S2, which shows that
275 the meteorological fields were faithfully reproduced in this study and can be used to drive the air quality model.
276

277 ISOP and monoterpene (TERP) are the major species of BVOC emission, making their concentration
278 assessment a feasible and convincing method for indirectly validating the accuracy of BVOC emission
279 estimates. [Table 2](#) ~~Table 2 delineated within this study~~ presents the mean concentrations of ISOP derived from
280 various cases juxtaposed with the observed average concentrations. This comparative analysis in the Modiesha
281 site reveals that after the incorporation of the UGS-BVOC emissions, there is an augmentation in the ISOP
282 concentration from 0.29 to 0.35 ppb and from 0.23 to 0.29 ppb under distinct land use cover cases (Gdef and
283 Ghr), relative to an observed concentration of 0.34 ppb. Meanwhile, the evaluation at the Wanqingsha site,
284 where the observed mean ISOP concentration was 0.45 ppb from September 7 to September 30, 2017, shows
285 that the modeled ISOP concentrations increased from 0.29 to 0.31 ppb and from 0.27 to 0.29 ppb under distinct
286 land use cover cases (Gdef and Ghr) when UGS-BVOC emissions were included. Additionally, all cases
287 successfully capture the hourly ISOP concentrations when compared to observations at both the Modiesha and
288 Wanqingsha sites (Figure S4). This increment signifies a substantial diminution in the discrepancy between
289 the modeled and observed concentrations attributable to the UGS-BVOC emissions. Analogously, the
290 integration of the UGS-BVOC emissions yields a refinement in the estimation accuracy of ISOP
291 concentrations at the Modiesha site, as evidenced by a reduced bias.

292
293 These findings reveal that ISOP concentrations are underestimated by 16.4% and 34.7% in the Modiesha and
294 Wanqingsha sites when UGS-BVOCs are excluded, respectively, suggesting the important role of UGS-
295 BVOCs emissions in modeling. Moreover, numerous studies highlight the significant role of ISOP in O₃
296 formation within the Pearl River Delta (PRD) region, including Guangzhou. For instance, Zheng et al., (2009)

demonstrated that ISOP has the highest ozone formation potential among all VOCs. Therefore, incorporating UGS-BVOCs into ISOP concentration estimates is crucial for accurately modeling regional O₃ levels.

Table 2 The evaluation results for the monthly mean ISOP concentrations. The “Gdef_N”, “Gdef_Y”, “Ghr_N”, and “Ghr_Y” columns show the various metrics from comparing the hourly observation and simulation values during September 2017 for the Modiesha site and 7 September 2017 to 30 September 2017 for the Wanqingsha site.

Site name	Metrics	Gdef_N (ppb)	Gdef_Y (ppb)	Ghr_N (ppb)	Ghr_Y (ppb)
Modiesha	Sim.	0.29	0.35	0.23	0.29
	Obs.	0.34	0.34	0.34	0.34
	MB	-0.06	0.01	-0.11	-0.05
	NME	76.0%	68.7%	73.6%	66.2%
	NMB	-16.4%	3.5%	-31.3%	-13.1%
	R	0.44	0.46	0.37	0.39
Wanqingsha	Sim.	0.29	0.31	0.27	0.29
	Obs.	0.45	0.45	0.45	0.45
	MB	-0.15	-0.14	-0.17	-0.15
	NME	58.9%	56.8%	60.4%	58.1%
	NMB	-34.7%	-30.6%	-38.7%	-34.8%
	R	0.35	0.39	0.34	0.4

Additionally, various statistical metrics were used to assess the performance of hourly O₃, MDA8 O₃, and NO₂ concentrations from the CMAQ simulation (Emery et al. 2017). These metrics comprise the correlation coefficient (R), normalized mean bias (NMB), and normalized mean error (NME). The formulas for these metrics are listed in Table S3. As shown in [Table 3](#), the modeling performance for all cases are reasonable, albeit with some degree of underestimation. Despite these discrepancies, the model demonstrates sufficient reliability and can be effectively used in the subsequent study. Meanwhile, the MBs of MDA8 O₃ across various cases indicate a substantial improvement in the CMAQ simulation when UGS-BVOC, UGS-LUCC, and their combined effects are considered. Specifically, the MB values of MDA8 O₃ decrease from -2.16 ppb in the Gdef_N case to -0.26 ppb in the Ghr_Y case, demonstrating that incorporating UGS-BVOC, UGS-LUCC, and their combined effects can enhance the accuracy of predicted daytime O₃ concentrations. In addition, we also evaluate the simulation performance for NO₂ in each case and the results suggest that all models have R above 0.63, and while there is some overestimation, the NMB is 15.0%, 15.2%, 13.0%, and 13.2% for Gdef_N, Gdef_Y, Ghr_N, and Ghr_Y, respectively. It should be emphasized that integrating UGS-BVOC into the [modeling process model](#) can slightly improve the accuracy of NO₂ predictions, reducing the MB from 3.27 to 3.24 ppb, and from 2.84 to 2.81 ppb for Gdef and Ghr cases, respectively. The improvement in NO₂ predictions is attributed to the inclusion of UGS-BVOC emissions in the CMAQ model, which

enhances NO₂ involvement in O₃ formation. This process leads to lower simulated NO₂ concentrations, reducing the MBs compared to observations.

Table 3 Evaluation results of the simulated monthly mean hourly O₃, MDA8 O₃, and hourly NO₂ mixing ratios for each case during September 2017.

Pollutant	Case name	Sim (ppb)	Obs (ppb)	MB (ppb)	NMB	NME	R
Hourly O ₃	Gdef_N	28.23	30.49	-2.26	-6.7%	23.6%	0.82
	Gdef_Y	28.67	30.49	-1.82	-5.3%	23.6%	0.82
	Ghr_N	28.89	30.49	-1.60	-4.8%	22.5%	0.83
	Ghr_Y	29.33	30.49	-1.15	-3.4%	22.4%	0.83
MDA8 O ₃	Gdef_N	60.11	62.27	-2.16	-3.47%	21.71%	0.84
	Gdef_Y	61.04	62.27	-1.23	-1.97%	21.40%	0.84
	Ghr_N	61.07	62.27	-1.20	-1.92%	21.28%	0.84
	Ghr_Y	62.00	62.27	-0.26	-0.42%	21.23%	0.84
Hourly NO ₂	Gdef_N	24.78	21.50	3.27	15.2%	45.7%	0.63
	Gdef_Y	24.74	21.50	3.24	15.0%	45.5%	0.63
	Ghr_N	24.35	21.50	2.84	13.2%	43.8%	0.63
	Ghr_Y	24.32	21.50	2.81	13.0%	43.6%	0.63

In terms of O₃, the UGS-BVOC, UGS-LUCC, and their combined effects have various performances in different regions (Table 4). These results indicate that the inclusion of UGS-BVOC emissions significantly influences MDA8 O₃ and hourly O₃ concentrations in the city center region and this effect, primarily observed when comparing the Gdef_Y with Gdef_N and Ghr_Y with Ghr_N cases, is largely due to the VOC-limited areas prevalent in Guangzhou (He et al., 2024). By integrating the UGS-BVOC emissions and UGS-LUCC into the models (comparing Ghr_Y and Gdef_N cases), the MBs of MDA8 O₃ and hourly O₃ in all regions, including a notable improvement in the city center region from -3.63 to -0.75 ppb and -2.86 to -1.52 ppb, respectively, is reduced. Additionally, the UGS-BVOC emissions slightly enhance R values of MDA8 O₃ and hourly O₃ in the city center and suburban regions, indicating a more accurate the daytime trend and the diurnal cycle representation, respectively. The UGS-LUCC effects, as seen when comparing Ghr_N and Gdef_N cases, also greatly improve model biases and the combined effects of both UGS-BVOC and UGS-LUCC (comparing the Ghr_Y and Gdef_N cases) substantially ameliorate model biases in the city center and suburban regions.

Table 4 Evaluation results of simulated monthly mean hourly O₃ and MDA8 O₃ mixing ratios in city center, suburban, and rural areas for each case during September 2017.

Variable	Regions	MB (ppb)				R			
		Gdef_N	Gdef_Y	Ghr_N	Ghr_Y	Gdef_N	Gdef_Y	Ghr_N	Ghr_Y
MDA8 O ₃	City center	-3.63	-2.24	-2.11	-0.75	0.81	0.81	0.81	0.81

	Suburban	-4.08	-3.25	-3.21	-2.38	0.74	0.74	0.72	0.73
	Rural	-5.11	-4.76	-4.87	-4.53	0.67	0.66	0.70	0.69
	City center	-2.86	-2.29	-2.09	-1.52	0.80	0.80	0.81	0.81
Hourly O ₃	Suburban	-3.15	-2.80	-2.65	-2.30	0.82	0.83	0.82	0.83
	Rural	-1.18	-1.63	-1.38	-1.16	0.74	0.74	0.75	0.75

3.2 Estimation of UGS-BVOC emissions under different land use cover

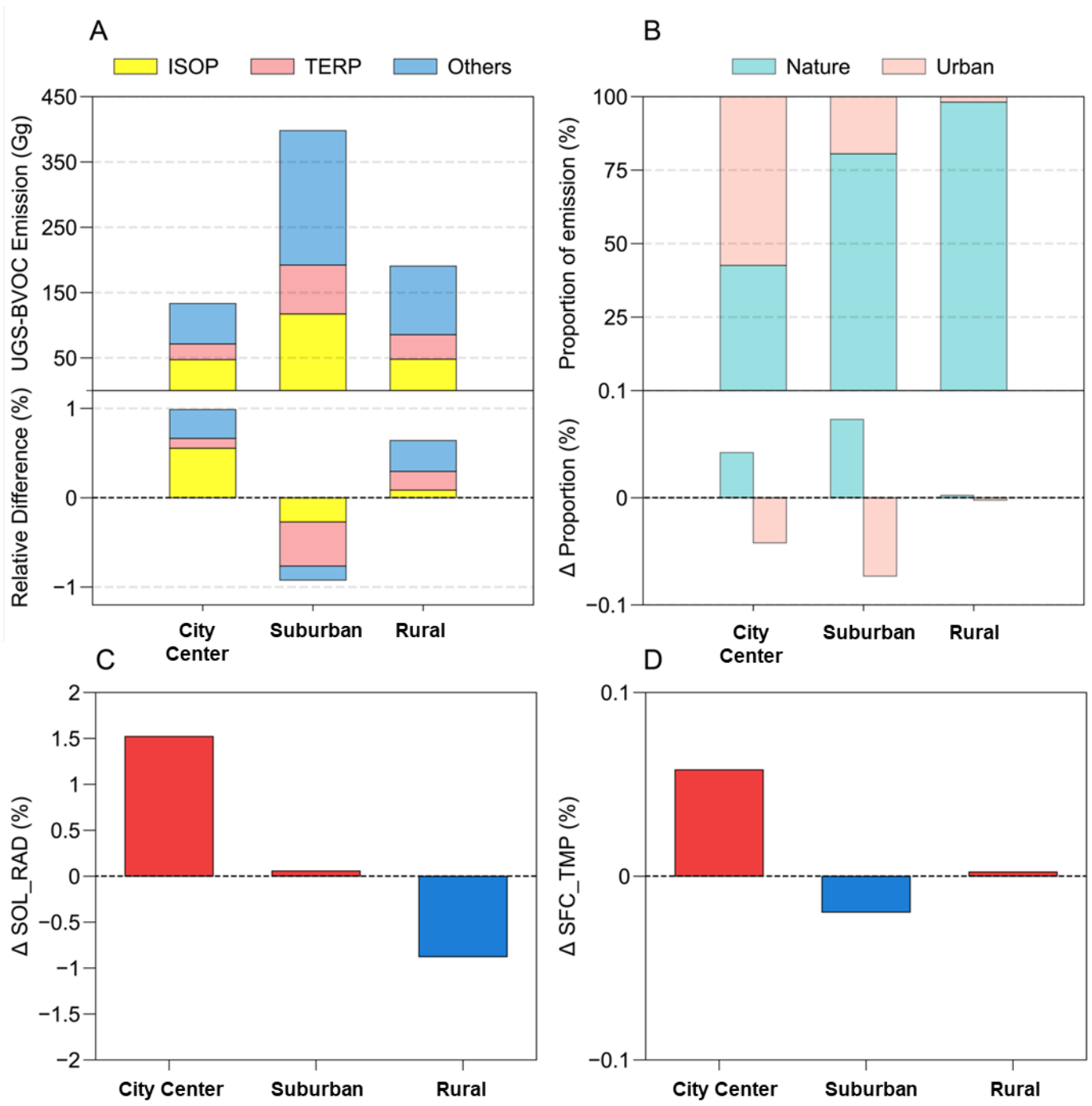
This study comprehensively summarizes the UGS-BVOC emissions across various species for all regions in Guangzhou City in September. Given that the variances in the UGS-BVOC emissions due to different land use covers are relatively minor, [the primary Table 5](#) presents emissions driven by the default land use cover. For a detailed breakdown of emissions attributable to varied land use covers, refer to Table S4. A review of the data reveals that TERP and ISOP rank as the [highest emitting species](#) with proportions are 20.46% and 31.91% in this study, respectively, aligning with the findings of previous studies (Cao et al., 2022; Guenther et al., 2012b). Furthermore, [Table 5](#) reveals that in September, the UGS-BVOC emissions in Guangzhou amounted to 666 Gg (~90 Mg/km²), with ISOP and TERP contributing remarkably to the total UGS-BVOC emissions. In comparison to anthropogenic VOC (AVOC) and BVOC emissions, UGS-BVOC emissions account for approximately 33.45% in the city center region. Regionally, the suburban region registered the highest UGS-BVOC emissions in Guangzhou, peaking at 367 Gg. This is followed closely by the rural and city center regions, recording emissions of 174 Gg and 126 Gg, respectively.

Table 5 The summarized table of UGS-BVOC emissions in Guangzhou city in September 2017 via default land use cover (units: Gg).

Species	Abbreviations	City center (Gg)	Suburban (Gg)	Rural (Gg)	Total (Gg)
Acetic acid	AACD	0.86	2.44	1.18	4.48
Acetaldehyde	ALD2	3.46	11.57	5.83	20.86
Formaldehyde	FORM	0.95	3.90	2.17	7.02
Methanol	MEOH	12.47	41.31	20.36	74.14
Formic acid	FACD	2.79	7.84	3.79	14.42
Ethane	ETHA	2.12	8.40	4.64	15.16
Ethanol	ETOH	3.63	12.13	6.11	21.87
Acetone	ACET	6.22	21.52	11.63	39.37
Propane	PRPA	2.08	8.21	4.54	14.83
Ethene	ETH	3.97	15.64	8.64	28.25
Isoprene	ISOP	47.30	117.32	48.06	212.68
Monoterpenes	TERP	24.07	74.85	37.51	136.43
Alpha pinene	APIN	11.26	30.07	13.16	54.49
Methane	ECH4	0.04	0.14	0.08	0.26
Sesquiterpenes	SESQ	4.31	11.97	5.95	22.23

Total	Total	125.53	367.31	173.65	666.49
-------	-------	--------	--------	--------	--------

356
357 [Figure 2Figure 2A](#) provides a detailed illustration of the UGS-BVOC emissions across various regions in
358 Guangzhou City, driven by default land use cover data, and compares these with the estimates derived from
359 high-resolution land use cover data, which presents that the suburban region exhibits the highest UGS-BVOC
360 emissions among the three studied regions, totaling 413.47 Gg. This predominance is linked to the larger
361 extent of UGS in the suburban region, as depicted in [Figure 3Figure 5A](#), while the emissions in the city center
362 and rural regions are reported at 137.69 Gg and 198.64 Gg, respectively. Moreover, UGS-LUCC is
363 instrumental in modulating BVOC emissions, leading to an uptick in the city center and rural regions while
364 precipitating a decline in the suburban region. Notably, a slight increase in solar radiation (SOL_RAD) by
365 0.05% ([Figure 2Figure 2C](#)), attributable to a reduced urban fraction in the Ghr dataset, results in augmented
366 solar exposure. Concurrently, a marginal reduction in surface temperature (SFC_TMP) by 0.02% ([Figure
367 2Figure 2D](#)), facilitated by increased vegetation albedo cooling effects, underpins the decrease in UGS-BVOC
368 emissions within suburban regions. This phenomenon underscores the critical role of lowered SFC_TMP—
369 driven by vegetation's higher albedo—in curtailing emissions stemming from UGS-LUCC. Temperature-
370 dependent BVOC emissions are among the well-known key temperature-dependent mechanisms influencing
371 ozone levels, alongside other processes including changes in chemical reaction rates, soil NO_x emissions, dry
372 deposition, and PAN decomposition, as demonstrated in Li et al. (2024). Moreover, in the city center contexts,
373 the diminished urban fraction enhances SOL_RAD and SFC_TMP, promoting higher emissions, a trend
374 mirrored to a lesser extent in the rural region following the update of land use cover data to Ghr. [Figure 2Figure
375 2B](#) offers a clear depiction of the proportion of UGS-BVOC emissions relative to non-UGS area BVOC
376 emissions in each region of Guangzhou City, which presents that the UGS-BVOC emissions in the city center
377 region constitute 57.34% of the total BVOC emissions in this region because of the larger urban proportions
378 in the city center region ([Figure 3Figure 5](#)), while the UGS-BVOC emission proportion in suburban and rural
379 are 19.44% and 1.86% respectively. This indicates a significant contribution of the UGS-BVOC emissions in
380 the the city center region. Furthermore, when examining the relative differences in the BVOC emissions
381 resulting from various land use covers across the city, the changes are found to be minimal, which suggests
382 that meteorological alterations from land use cover do not majorly influence the proportion of the UGS-BVOC
383 emissions emanating in Guangzhou. Thus, factors other than land use changes might be more critical in
384 shaping the distribution and intensity of the UGS-BVOC emissions in urban settings.



385
 386 Figure 2 (A) The UGS-BVOC emissions of each species (upper panel) and relative difference (Ghr - Gdef) from various land use cover
 387 (lower panel), (B) the proportion of the BVOC emissions from urban and nature areas (upper panel) and the relative proportion
 388 difference (Ghr - Gdef) from various land use cover (lower panel), (C) the relative difference of solar radiation (C), and (D) surface
 389 temperature in each region (D) driven via various land use cover datasets. All values in these figures are during September 2017.
 390

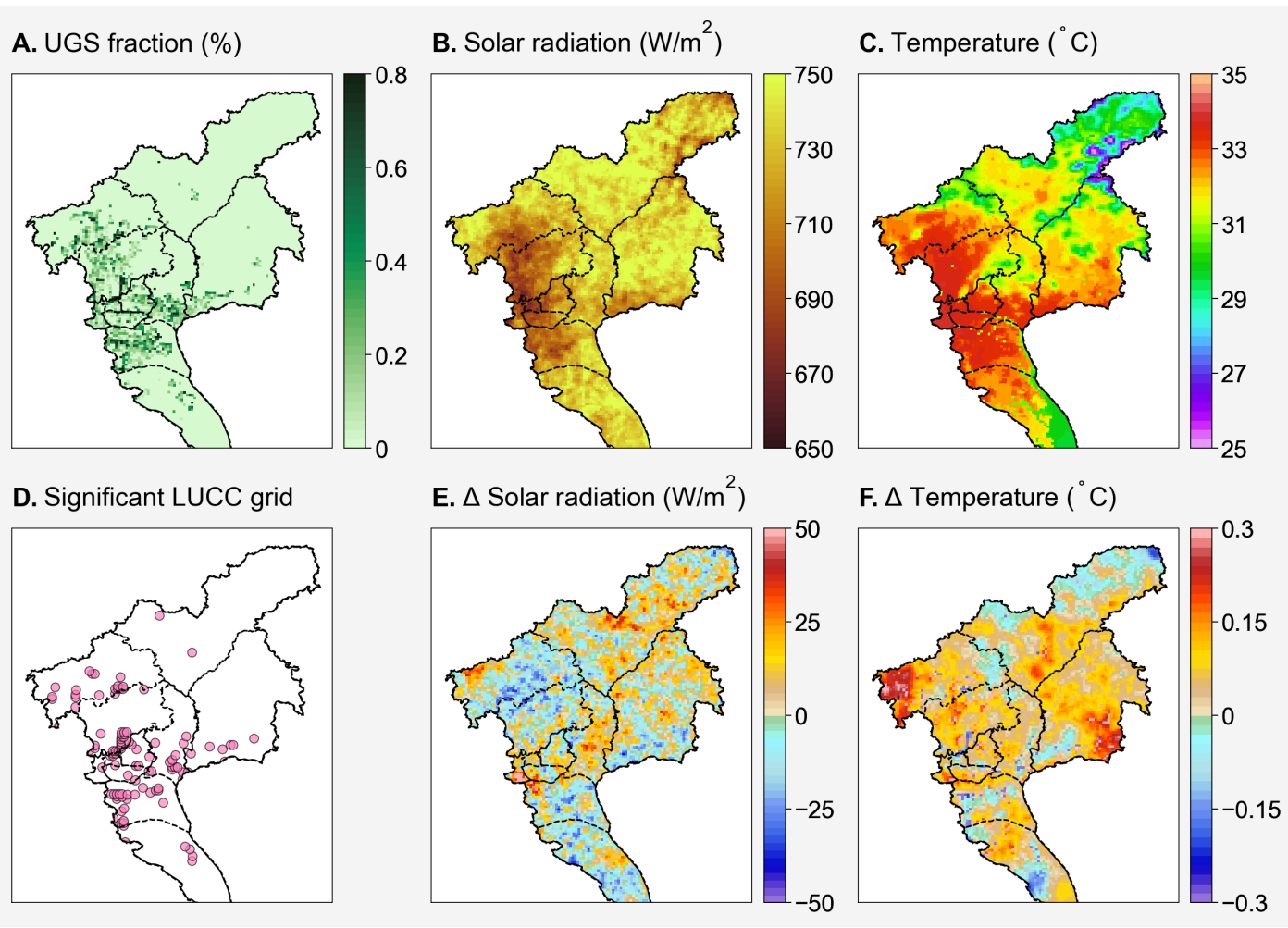
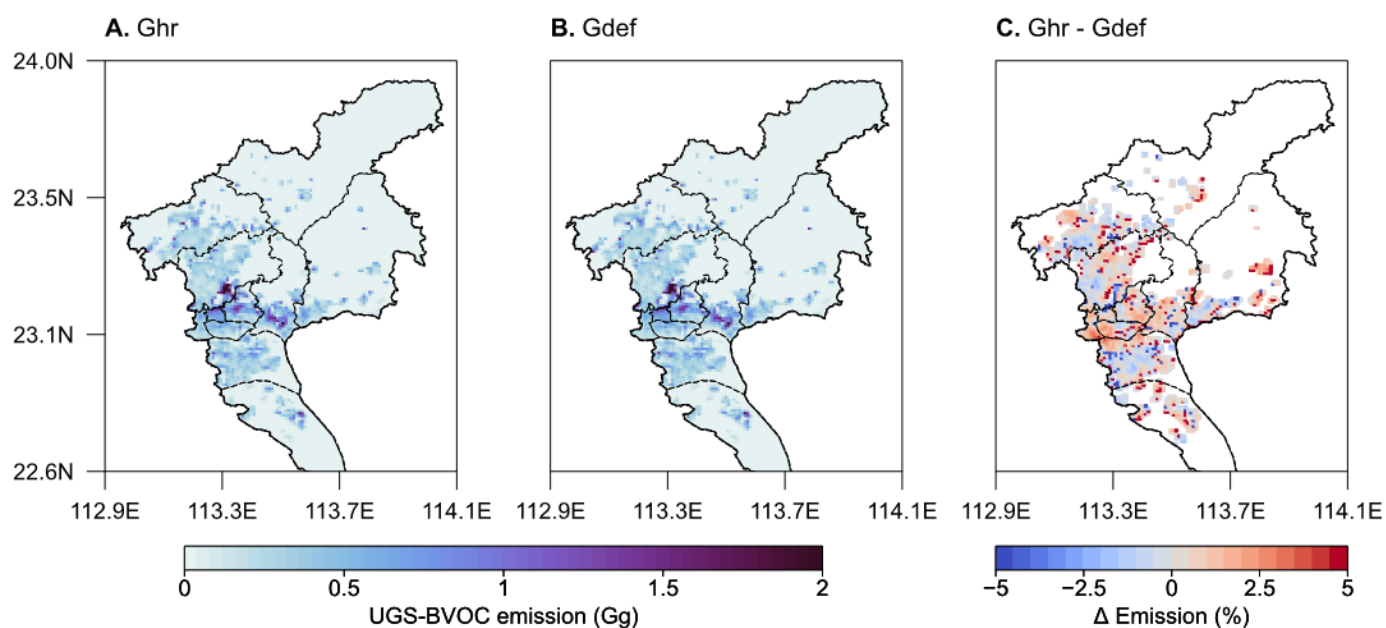


Figure 35 The UGS map (A) and the meteorological fields during September 2017 from the Ghr - N case (B and C). (D) is the grid locations where the land use experienced significant changes. (E) and (F) are the differences in solar radiation and temperature during the analysis periods (1 September 2017 to 30 September 2017) in various land use cover data (Ghr - Gdef).

Figure 3A-B collectively highlight the patterns of the UGS-BVOC emissions across different land use covers, pinpointing the emission hotspots in city center and suburban regions, which effectively illustrate how land use cover influences the UGS-BVOC emissions in various parts of the city. Additionally, Figure 3C delves into the disparities in the UGS-BVOC emissions attributed to different land use cover datasets. It reveals that the variations in emissions are predominantly concentrated in the identified hotspots. Moreover, Figure 3C indicates that employing high-resolution land cover data typically results in marginally higher estimates of the UGS-BVOC emissions, with an increase ranging between 0.8% to 2.9%. Figure 5E-F illustrate that despite a marginal reduction in solar radiation within the city center region, a corresponding minor temperature elevation modestly boosts UGS-BVOC emissions, which presents that the increase in temperature from UGS-LUCC causes the rise of the UGS-BVOC emissions.



407
 408 **Figure 43** The UGS-BVOC emission maps in September 2017 from default (A) and high-resolution (B) land use cover, and the differences
 409 of various UGS-BVOC emissions (C).
 410

411 As illustrated in Figure S1, UGS in Guangzhou comprises three primary types of vegetation: evergreen
 412 broadleaf forests, which are composed of Evergreen Broadleaf Trees (EBTs), cropland, and grasslands. This
 413 classification has enabled a more nuanced understanding of how different types of UGS vegetation influence
 414 UGS-BVOC emissions. [Figure 5](#) ~~Figure 4~~ reveals that EBTs predominate the urban vegetation landscape in
 415 Guangzhou and are associated with higher rates of UGS-BVOC emissions as their coverage increases.
 416 Conversely, an increase in the proportion of cropland correlates with reduced UGS-BVOC emissions,
 417 highlighting its minimal contribution to the overall UGS-BVOC emissions of Guangzhou. Grasslands exhibit
 418 a variable impact on BVOC emissions; when they constitute over 80% of the UGS, the emission rates are
 419 relatively low. However, when grassland coverage ranges between 60-80%, its BVOC emissions surpass those
 420 from cropland within the same percentage range. Overall, EBTs emerge as the primary contributors to UGS-
 421 BVOC emissions, with grasslands and croplands making lesser contributions.

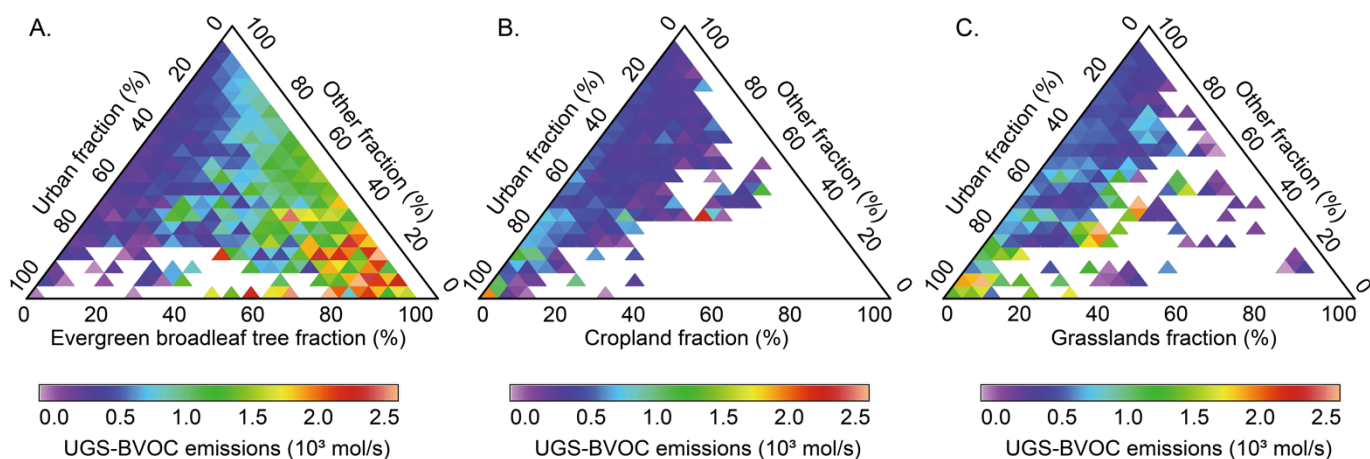
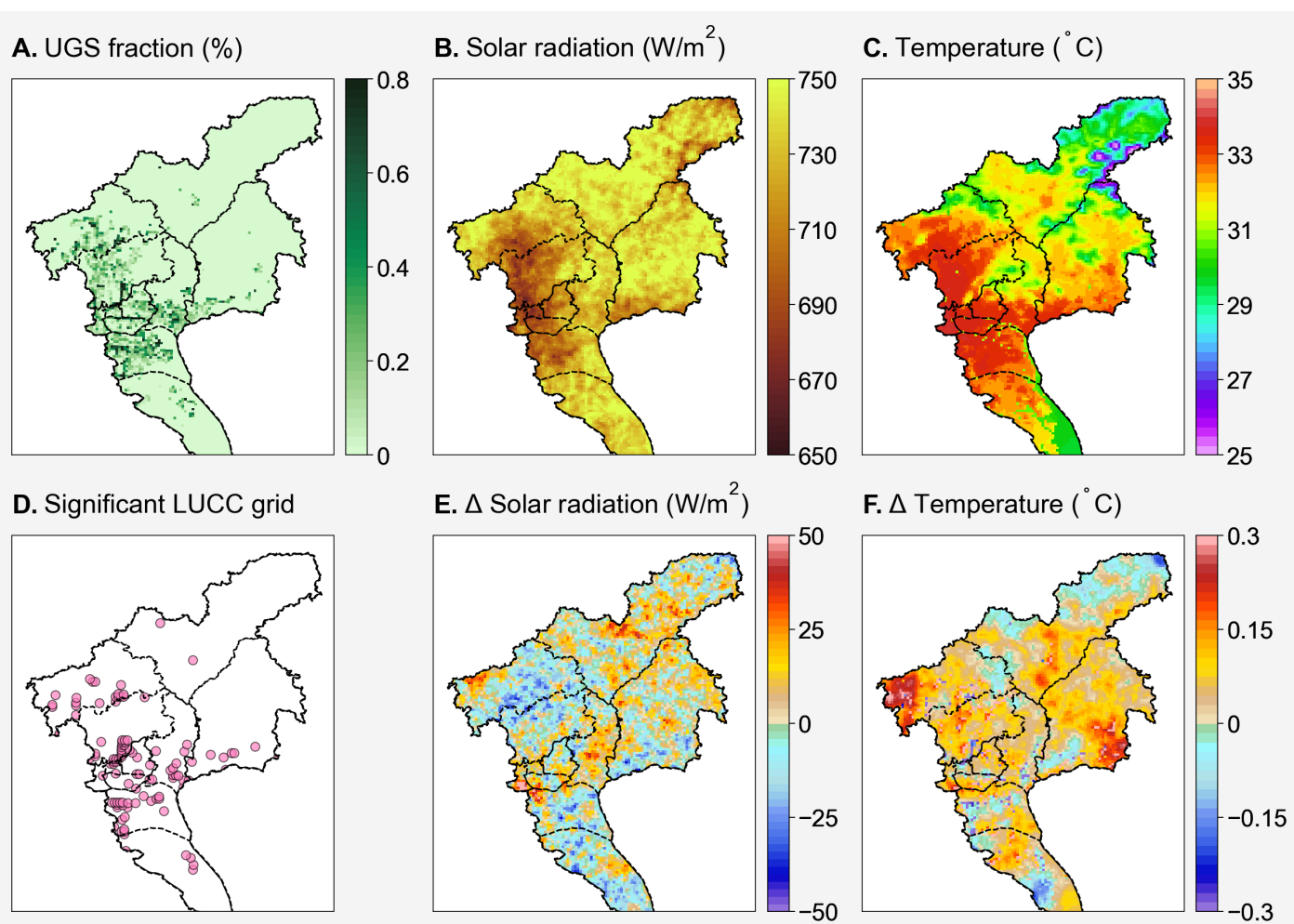


Figure 54 Ternary heat map for various vegetation in UGS with the UGS-BVOC emission rate and the invalid value in this figure represents no UGS-BVOC emission.

In addition to the proportion of UGS, the UGS-BVOC emissions in Guangzhou city are significantly influenced by meteorological factors such as surface temperature and solar radiation (Guenther et al., 2020b). To elucidate the spatial heterogeneity of the UGS-BVOC emissions, this study analyzes variations in these key factors. The simulation results depicted in Figure 3Figure 5A show the distribution pattern of UGS, which are predominantly located in the city center region, which account for a higher percentage of the UGS-BVOC emissions compared to others. Interestingly, as indicated in Figure 3Figure 5B, the city center region receives less solar radiation than other regions likely due to the shading effect of urban canopies. Conversely, the city center region exhibits elevated temperatures attributable to the urban heat island effect, leading to an increase in UGS-BVOC emissions. Thus, while the distribution of UGS contributes to the variation in the UGS-BVOC emissions across different regions, the more significant factor is the enhanced UGS-BVOC emission due to higher temperatures in densely urbanized areas. The spatial dynamics of the UGS-BVOC emissions are significantly shaped by two key meteorological factors: solar radiation and surface temperature. These elements independently play a crucial role in determining both the spatial pattern and the intensity of the UGS-BVOC emissions. Solar radiation directly influences the rate of photosynthesis and, consequently, the production of BVOCs, while temperature affects not only the physiological processes of vegetation but also the volatilization rate of these compounds (Fuhrer et al., 1997; Lombardozzi et al., 2015). The intricate interplay between these factors leads to spatial variations in the UGS-BVOC emissions, with areas receiving higher solar radiation and experiencing warmer temperatures typically exhibiting more intense BVOC emissions.



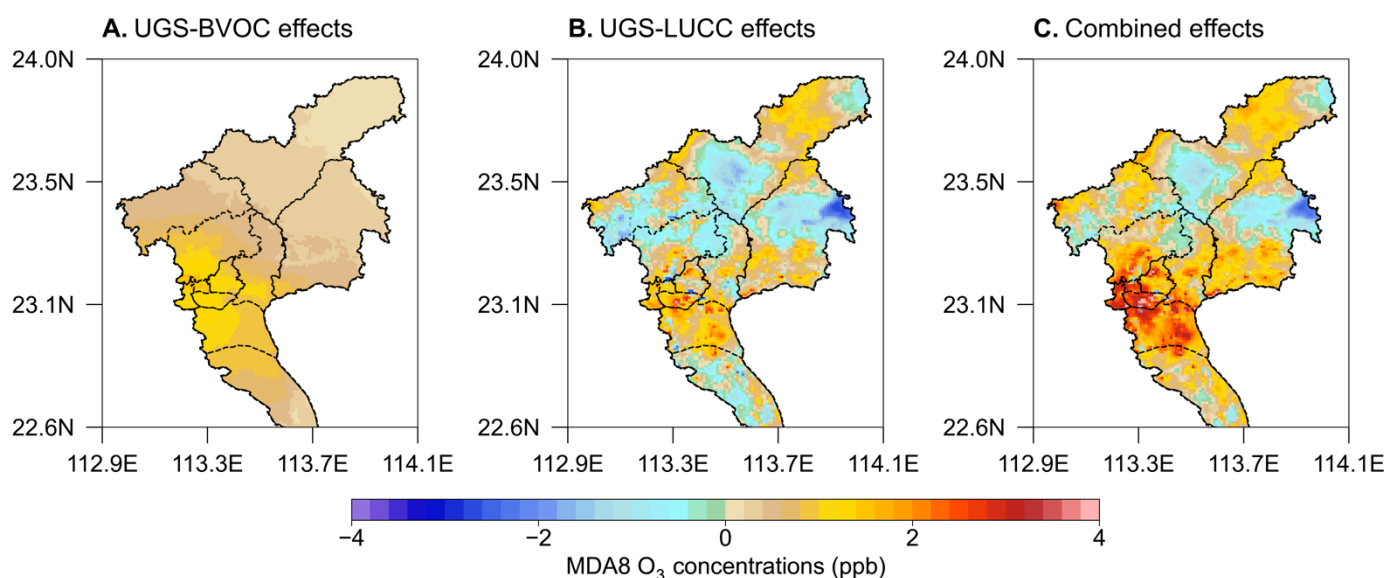
446 **Figure 5** The UGS map (A) and the meteorological fields during September 2017 from the Chr_N case (B and C). (D) is the grid locations
 447 where the land use experienced significant changes, (E) and (F) are the differences in solar radiation and temperature during the analysis
 448 periods (1 September 2017 to 30 September 2017) in various land use cover data (Chr_Gdef).
 449

450 This section has conclusively demonstrated that during the high O_3 season (September) in Guangzhou, the
 451 contribution of UGS-BVOC is substantial and cannot be overlooked and a notable finding is the strong spatial
 452 heterogeneity in these emissions across the city. The analysis also highlights high-resolution land use cover
 453 data increase the estimation of the UGS-BVOC emissions in the city center region.

454 3.3 Impact of UGS-LUCC and UGS-BVOC on Ozone Concentrations

455 The study evaluates the effects of UGS-BVOC and UGS-LUCC on MDA8 O_3 concentrations in Guangzhou,
 456 both individually and in combination. [Figure 6](#) presents the absolute contributions from various cases,
 457 while the relative differences are shown in Figure S5. The analysis reveals that the UGS-BVOC emissions
 458 alone ([Figure 6A](#)) primarily affect the city center region, greatly increasing MDA8 O_3 concentrations
 459 by 1.0-1.4 ppb (+2.3-3.2%), which increment aligns with findings from Los Angeles, where Schlaerth et al.,
 460 (2023) reported a contribution of 1.2 ppb from UGS-BVOC to urban MDA8 O_3 levels. N. Wang et al. (2019)

461 reported that VOC levels can be highly sensitive in VOC-limited regions, where sufficient NO_x concentrations
 462 mean that even a small disturbance in VOCs can cause significant changes in O₃ concentrations. Similarly,
 463 metropolitan areas, such as Guangzhou, often experience VOC-limited conditions or NO_x-saturation (P. Wang
 464 et al., 2019). Consequently, the UGS-BVOC case results in an overall increase in MDA8 O₃. In contrast, the
 465 sole impact of the UGS-LUCC effects (Figure 6B) is more extensive, influencing both the city center
 466 and suburban regions and resulting in a general increase of approximately 1.1-2.0 ppb (+2.3-4.3%) in MDA8
 467 O₃ levels, which can be attributed to the higher temperature and solar radiation (Figure 3E-F). In
 468 Guangzhou, the transformation of urban surfaces to natural vegetation due to UGS-LUCC results in lower
 469 albedo and consequently lower temperatures. However, this change also reduces the height of the urban canopy,
 470 diminishing its shading effects on solar radiation and paradoxically leading to higher temperatures in some
 471 regions. Therefore, considering the UGS-LUCC effect, the decreased urban canopy height could lead to
 472 elevated temperatures, thereby potentially increasing ozone production. However, the most significant results
 473 emerge under the combined effect of UGS-BVOC and UGS-LUCC (Figure 6C), where a substantial
 474 increase in O₃ concentration, ranging from 1.7-3.7 ppb (+3.8-8.5%), is observed across both the city center
 475 and suburban regions. The observed increase suggests a potentially significant influence of UGS-BVOC
 476 emissions and UGS-LUCC on ozone levels, indicating that these factors may play an important role in ozone
 477 pollution research and should be carefully considered. This finding underscores the essential role that
 478 integrated urban planning and environmental management play in controlling ozone pollution within
 479 metropolitan regions. By considering UGS-BVOC emissions in air quality models and management plans,
 480 managers can make more informed decisions to mitigate ozone levels and improve regional air quality.



481
 482 **Figure 6** The map of UGS-BVOC effects (a), LUCC effects (b), and combined effects (c) in MDA8 O₃. Each map shows the difference in

483 average MDA8 O₃ concentrations for each case (Gdef_Y, Ghr_N, and Ghr_Y) relative to the Gdef_N case during September 2017.

484
485 Previous studies have established that O₃ episodes are often accompanied by high temperatures and intense
486 solar radiation, conditions that can exacerbate the UGS-BVOC emissions, critically affecting air quality model
487 performance (Shan et al., 2023; Soleimanian et al., 2023). In this study, an O₃ episode is defined as a period
488 of two or more consecutive days with MDA8 O₃ concentrations exceeding 160 µg/m³ (~80 ppb) (Wu et al.,
489 2020). Our analysis, as depicted in [Figure 7](#)~~Figure 7~~A, identified two such episodes in Guangzhou City during
490 September: the first from September 16 to 21 and the second from September 26 to 28. The Gdef_N case
491 successfully captures these episodes but tends to underestimate both MDA8 O₃ during these episodes. [Figure](#)
492 ~~7~~[Figure 7](#)B-C highlight a notable reduction in wind speed during both episodes, particularly during the second
493 episode. Despite some diffusion enhancement due to increased PBLH with rising surface temperatures (Figure
494 S6), the surface temperature hike concurrently fosters O₃ production. Consequently, the episodes were
495 dominated by a combination of temperature increases, which elevated O₃ concentrations, and wind speed
496 decreases. Furthermore, [Figure 7](#)~~Figure 7~~C illustrates that there was a significant spike in carbon monoxide
497 (CO) concentrations during these episodes. CO, often used as a tracer in studies, indicates the worsening of
498 diffusion conditions, leading to the accumulation of NO₂ - a primary O₃ precursor - thereby culminating in O₃
499 episodes in Guangzhou city.

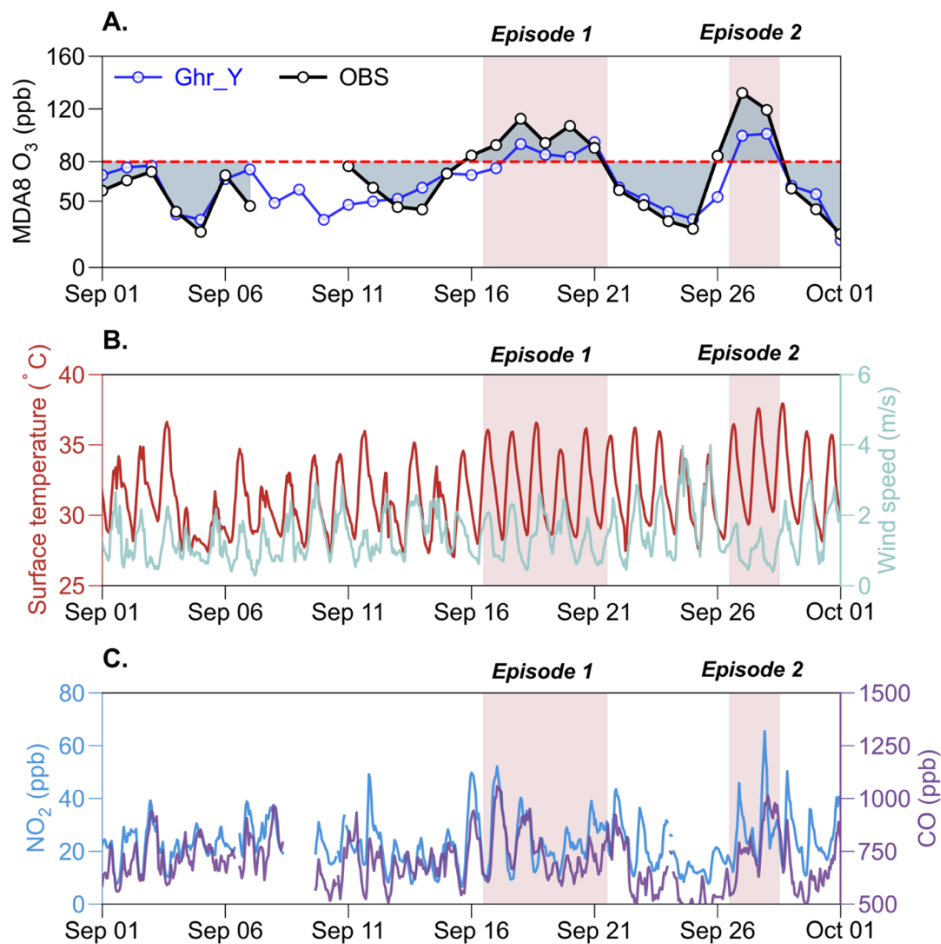


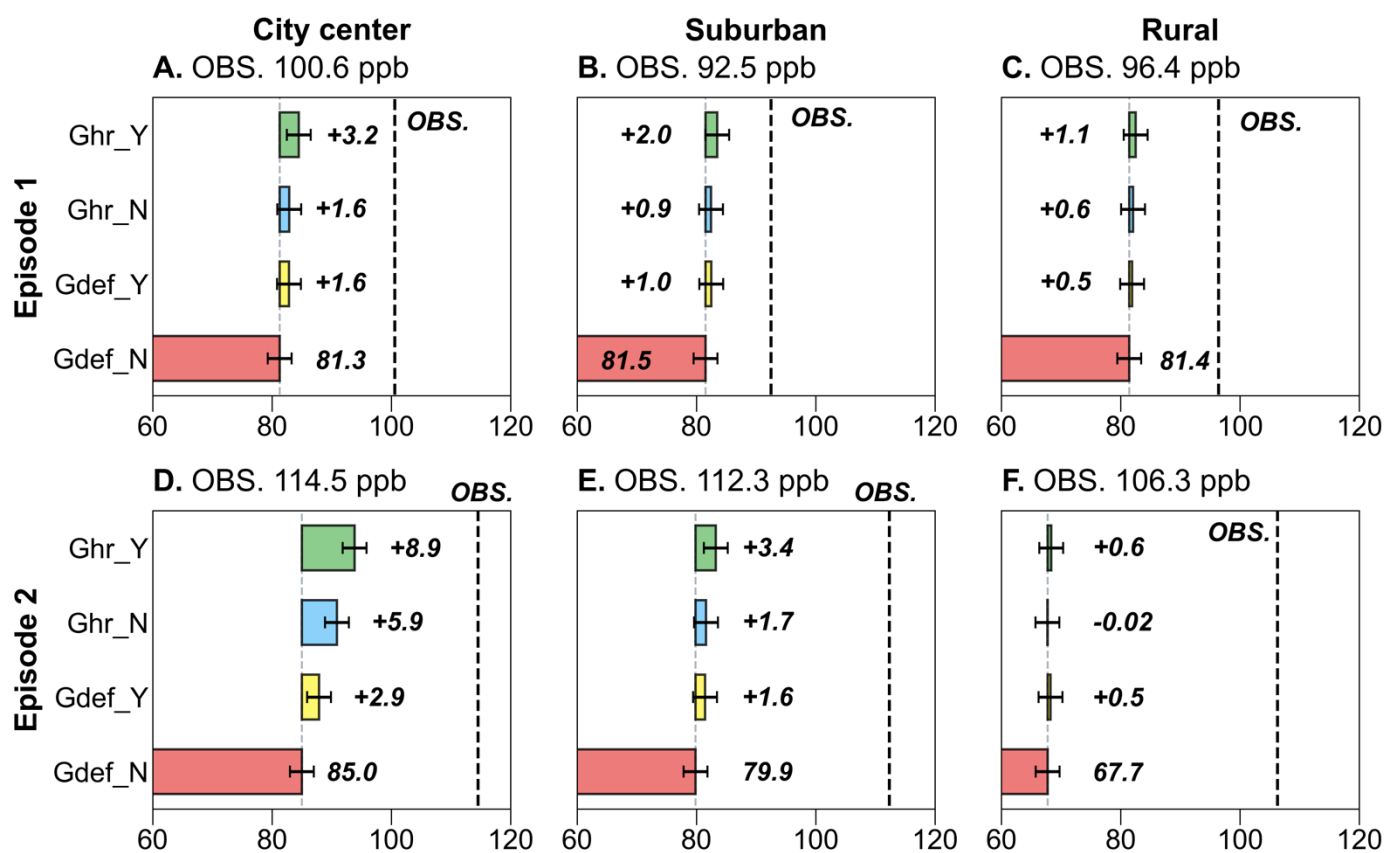
Figure 7 The comparison during September 2017 between the average values from simulation results grids which have air quality stations produced by the Gdef_N case and the average observation values for MDA8 O₃ (A). (B) are the meteorological fields from the average values from the simulation result grids, which have the same locations as the air quality stations. (C) are the observed average values for NO₂ and CO concentrations from all air quality stations.

Figure 8 presents the assessment of O₃ episode simulations. The Gdef_N case initially underestimated O₃ concentrations, leading to an evaluation of improvements using three cases: UGS-LUCC (Ghr_N), UGS-BVOC emissions (Gdef_Y), and their combined effects (Ghr_Y).that in assessing the simulation of O₃ episodes, the Gdef_N case, which initially underestimated O₃ concentrations, prompted an evaluation of improvements using different cases: UGS-LUCC (Ghr_N), UGS-BVOC emissions (Gdef_Y), and a combination of both (Ghr_Y). The analysis, focusing on the city-center, suburban, and rural stations, reveals that all cases tend to underestimate O₃ levels between both episodes. However, incorporating the UGS-BVOC emissions into the model results in a notable increase in mean simulated MDA8 O₃ concentrations, particularly in the city center and suburban regions. For the sites in the city center region, the mean simulated MDA8 O₃ increased by +1.6 and +2.9 ppb (+1.8% and +3.3%, respectively), while for suburban sites, the increase was +1.0 ppb (+1.1%) and +1.6 ppb (+1.9%), with rural sites experiencing a smaller increase of only +0.5 ppb (+0.5%) and +0.5 ppb (+0.7%). This trend indicates a more pronounced impact in the city center and suburban

518 regions compared to the rural region. Notably, the influence of the UGS-BVOC emissions on MDA8 O₃ in
 519 Episode 2 (+2.9 ppb) was significantly greater than in Episode 1 (+1.6 ppb), suggesting that meteorological
 520 conditions in Episode 2 were more conducive to the UGS-BVOC emissions, particularly in the city center
 521 region, which usually is VOC-limited areas.

522

523 In Episode 1, the UGS-LUCC effects on O₃ concentrations were comparable to that of UGS-BVOC emissions,
 524 but in Episode 2, the UGS-LUCC effects led to a near doubling of urban MDA8 O₃ increase by 5.9 ppb
 525 (+6.48%) compared to the UGS-BVOC emissions. This indicates that the UGS-LUCC effects play a non-
 526 negligible role in O₃ pollution studies, and the response to such changes under different meteorological
 527 conditions varies significantly. Furthermore, due to the limited proportion of UGS in suburban and rural areas,
 528 the increased effect of UGS on O₃ is less pronounced in these regions, and nearly negligible in Episode 2.
 529 While the UGS-BVOC emissions alone have a modest effect on O₃ concentrations, their impact can become
 530 significant when combined with the UGS-LUCC effects. For instance, the combined effects in the city center
 531 region increased by 3.2 ppb (+3.7%) and 8.9 ppb (+10.0%) during Episode 1 and Episode 2, respectively.



532

533

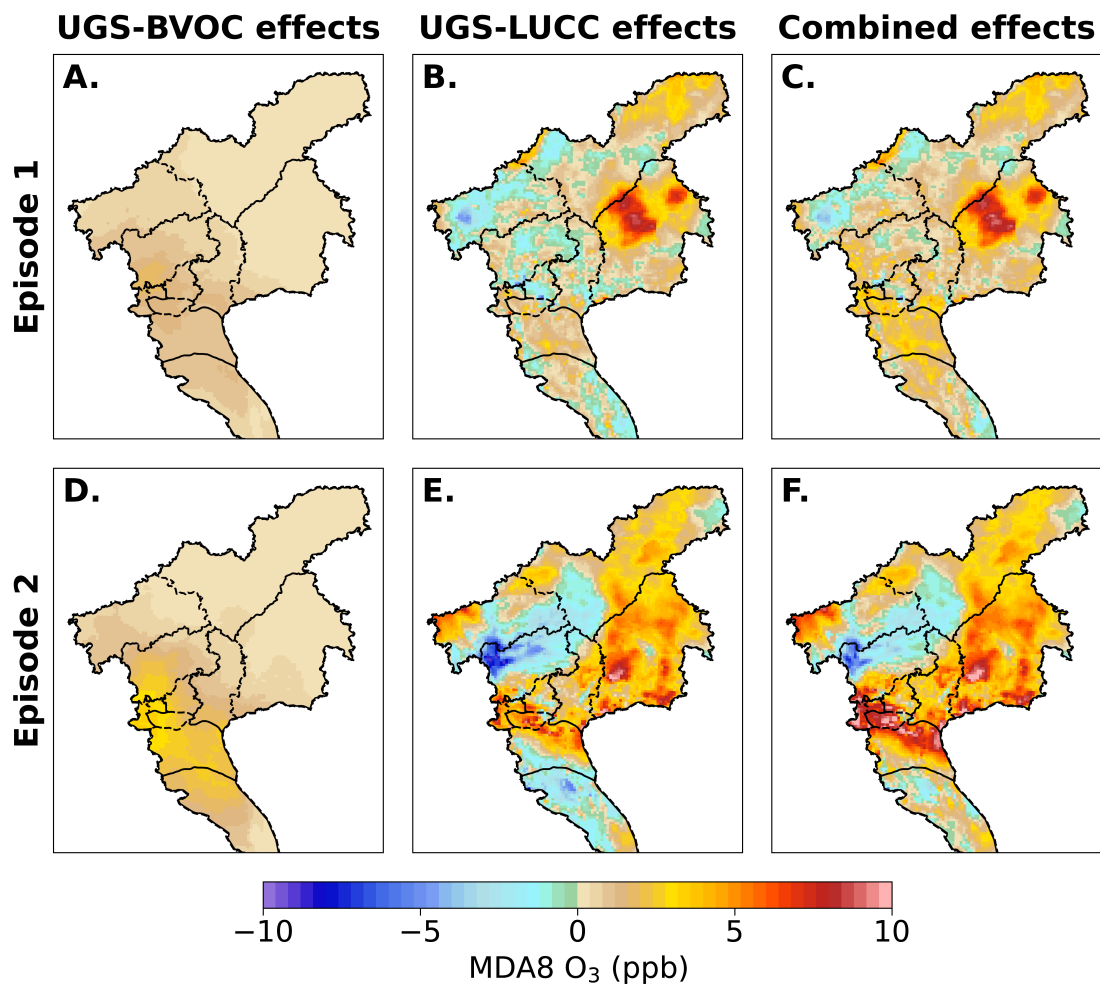
534

535

536

Figure 8 Comparison of simulated versus observed mean MDA8 O₃ concentrations across different cases for two episodes. The figure is organized into columns representing city center (4 sites), suburban (3 sites), and rural (2 sites) settings (columns 1-3, respectively) and rows indicating comparisons for episode 1 and episode 2 (rows 1 and 2, respectively).

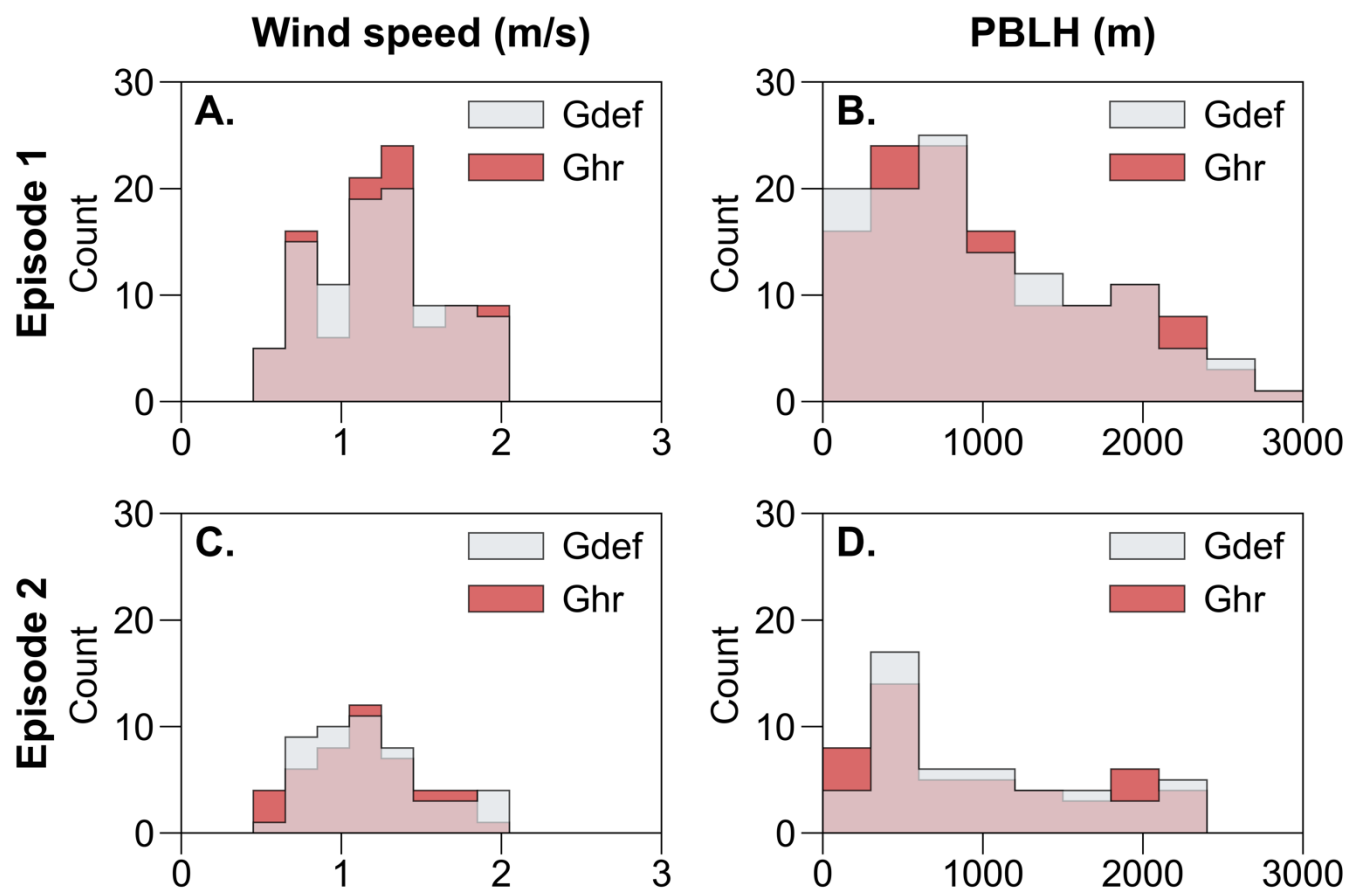
537 [Figure 9](#) presents the map of each effect on MDA8 O₃ in both episodes and the influence of UGS-
538 BVOC emissions ([Figure 9A](#) and [Figure 9D](#)) on the MDA8 O₃ concentration during Episode
539 1 and Episode 2 ranges from 0 to 2.0 ppb and 0 to 3.5 ppb, respectively, with the city center region witnessing
540 the most significant impact. This variance can be primarily ascribed to the heightened temperatures during
541 Episode 2 ([Figure 7B](#)), which create conditions more conducive to ozone generation through UGS-
542 BVOC emissions. Furthermore, the UGS-LUCC effect's maximal contribution to the urban MDA8 O₃ levels
543 could escalate to 2.2 ppb in Episode 1 and 23.7 ppb in Episode 2 while the combined effects of UGS-LUCC
544 and UGS-BVOC emissions are projected to enhance MDA8 O₃ concentrations to 4.8 ppb and 25.2 ppb for the
545 respective episodes. This marked increase in the episodes' contributions can be linked to the differential
546 responsiveness of land use data under various meteorological conditions. Notably, while the contribution from
547 the UGS-BVOC effect during Episode 2 substantially exceeds that of Episode 1, the incremental impact of
548 UGS-LUCC on combined effects in Episode 2 is notably smaller than in Episode 1. This phenomenon
549 indicates that the escalated UGS-BVOC emissions in Episode 2 may start to inhibit ozone production rates
550 incrementally.



551
 552 **Figure 9** The UGS-BVOC effects (A, D), the UGS-LUCC effects (B, E), and the combined effects (C, F) in Episode 1 and Episode 2,
 553 respectively.

554
 555 [Figure 8](#) reveals that both observed O₃ episodes were primarily caused by reduced diffusion conditions.
 556 Notably, the impact of the UGS-LUCC effects varied significantly between the two episodes. Analysis of
 557 meteorological variables, specifically wind speed and PBLH, which are crucial for diffusion, demonstrate
 558 distinct patterns. [Figure 10](#) illustrates that during Episode 1, the UGS-LUCC effects led to a notable
 559 increase in the frequency of higher wind speeds (1.2–1.4 m/s) and a simultaneous decrease in the frequency
 560 of lower wind speeds (0.9–1.1 m/s). This shift in the wind speed distribution suggests an overall increase in
 561 average wind speed due to the UGS-LUCC effects during Episode 1. In contrast, Episode 2 experiences a
 562 significant decrease in wind speed frequency at 0.7-1.1 m/s, with an increase in the lower range of 0.5-0.7 m/s.
 563 This suggests that the UGS-LUCC effects further reduce the already low wind speeds in Episode 2.
 564 Concerning PBLH, the UGS-LUCC effects are observed to elevate PBLH during Episode 1, which led to a
 565 decrease in PBLH during Episode 2. Therefore, the UGS-LUCC effects are markedly more pronounced in
 566 Episode 2 than in Episode 1, contributing to a more substantial alteration of meteorological conditions

567 affecting air dispersion and, consequently, O₃ formation.



568
569 **Figure 10** The frequency of wind speed (column 1) and PBLH (column 2) in Episode 1 (row 1) and Episode 2 (row 2) driven by different
570 land use cover datasets.

571
572 [Table 6](#) ~~Table-6~~ presents the overall results for the impacts of UGS-LUCC and UGS-BVOC on MDA8 O₃
573 concentrations. The effects show slight variations across different regions during September, while the effects
574 during the two episodes exhibit more significant changes. In the city center region, which shows the largest
575 changes, the UGS-BVOC effect shows increases by +1.6 ppb in Episode 1 and +5.9 ppb in Episode 2,
576 indicating that the UGS-BVOC effects influence MDA8 O₃ concentrations in the city center during ozone
577 episodes, while their impact is minimal in suburban and rural regions. These results highlight the important
578 effects of UGS-LUCC and UGS-BVOC in urban areas, especially during O₃ pollution periods.

579 **Table 6** Summary of Average MDA8 O₃ Concentrations (ppb) for Various Effects during September 2017.

Regions	Periods	UGS-BVOC effect	UGS-LUCC effect	Combined effect
City center	Monthly	+0.4	0.0	0.4
	Episode 1	+1.6	+1.6	+3.2
	Episode 2	+2.9	+5.9	+8.9
Suburban	Monthly	+0.4	0.0	0.4
	Episode 1	+1.5	+0.9	+2.0
	Episode 2	+1.6	+1.7	+3.4
Rural	Monthly	+0.4	0.0	0.4

Episode 1	+0.5	+0.6	+1.1
Episode 2	+0.5	0.0	+0.5

4. Uncertainties and Limitations

In this study, we used land use and land cover data integrated at 1 km and 10 m resolutions to define the urban boundary and characterize the spatial distribution of UGS in Guangzhou. Additionally, we incorporate high-resolution LAI data, obtained through machine learning, as input for the MEGAN model. Using the WRF-CMAQ model, we quantify the effects of UGS BVOC, UGS LUCC, and their combined impacts on ozone concentrations in Guangzhou. However, some uncertainties and limitations remain.

First, the 10 m resolution land use and land cover data still cannot fully capture the spatial pattern of UGS in Guangzhou. As shown in Figure S2, although UGS in Guangzhou is primarily composed of EBTs, most of these EBTs are distributed along urban edges. This may result from distortions in the definition of urban extent, such as misclassifying mixed urban-vegetation grids as urban grids, caused by the coarse resolution of the 1 km land use and land cover data. The fuzzy definition of urban boundaries could lead to non-UGS areas being misclassified as UGS, potentially resulting in an overestimation of UGS BVOC emissions.

Second, due to resolution limitations, only larger patches of grassland, cropland, and woodland are recognized as UGS, while smaller UGS vegetation, such as street trees, often goes undetected at a 10 m resolution. This omission can lead to an underestimation of the UGS BVOC emissions.

Third, the 10 m and 1 km resolution land use and land cover data, along with the growth forms and ecotype data, use simplified categorizations for grids, which cannot fully capture the diversity of vegetation species within UGS. Since different vegetation species have varying emission factors, this simplification introduces some errors. Similarly, the oversimplified classification of land grids limits this study's ability to provide specific planning strategies for UGS at the species level. Nevertheless, it can highlight the importance of considering UGS BVOC and UGS LUCC in air pollution prevention and control policies.

Finally, Guangzhou, the study area, is a highly urbanized Chinese metropolis with a VOC limited region (Gong et al., 2018; Liu et al., 2018; Zhou Kai et al., 2011). As a result, even a relatively small amount of VOC

emissions, such as those from UGS BVOC, can significantly impact ozone concentrations. Therefore, policymakers in Guangzhou should prioritize addressing the role of UGS BVOC emissions in air pollution prevention and control. In other cities, particularly those with advanced urban development, high NO_x emissions often resulting from factors like high motor vehicle ownership can lead to VOC limited conditions. In such areas, it is equally important to emphasize the role of UGS BVOC emissions in ozone pollution. In contrast, cities with lower NO_x emissions identified as NO_x limited regions may experience minimal impact from UGS BVOC emissions on ozone concentrations.

4.5. Conclusion

The rapid urbanization process is accompanied by a higher frequency of ozone episodes. It has been increasingly recognized that UGS can potentially exacerbate ozone pollution under specific conditions due to the UGS-LUCC and UGS-BVOC emissions. Guangzhou, located in southern China and known as a pioneer city in reform and opening-up policies, has experienced rapid urbanization over the past thirty years, leading to increased challenges with ozone pollution. Despite efforts to reduce anthropogenic emissions, ozone episodes occur with relatively high frequency in Guangzhou. This study selected September 2017, a month with a high incidence of ozone episodes in Guangzhou, to estimate the UGS-BVOC emissions using the WRF-MEGAN model and quantitatively assess the impact of UGS-LUCC, UGS-BVOC, and their combined effects on two ozone episodes in September 2017 using the CMAQ model. The major findings are shown as follows.

1. In September 2017, the UGS-BVOC emissions in Guangzhou totaled 666 Gg, with ISOP and TERP as the major species, emitting 213 and 136 Gg, respectively. Spatially, UGS-BVOC emissions were predominantly located in the city center region, attributed to the more extensive distribution of UGS there. The study also indicates that meteorological changes caused by UGS-LUCC do not significantly affect UGS-BVOC emissions. Instead, the formation of emission spatial distribution and intensity is closely related to local surface temperature and solar radiation. This understanding underscores the importance of considering local solar radiation and temperature conditions when assessing and modeling the distribution of the UGS-BVOC emissions, as they are pivotal in driving the spatial characteristics of these emissions.
2. Considering the UGS-BVOC and UGS-LUCC effects can effectively mitigate the underestimation of

637 surface ozone concentrations by regional air quality models, though other factors such as inaccuracies
638 in emissions inventories, chemical mechanisms, and meteorological inputs may also contribute to these
639 underestimations. For instance, incorporating UGS-BVOC emissions results in an increase in ISOP
640 concentration from 0.29 ppb to 0.35 ppb and from 0.23 ppb to 0.29 ppb under different land use cases
641 (Gdef and Ghr), compared to a observed concentration of 0.34 ppb. This significant enhancement in
642 ISOP concentrations—the predominant component in BVOCs and the most crucial VOC for O₃
643 formation in the PRD—highlights two key points. Firstly, it indicates an improvement in the accuracy
644 of BVOC concentration simulations. Secondly, this precise estimation of BVOCs and the consideration
645 of UGS-LUCC has notably shifted the MB of MDA8 O₃ simulations from -3.63 ppb to -0.75 ppb in
646 the city center region. Additionally, the simulation of NO₂ concentrations also shows slight
647 improvements, with the MB decreasing from 3.27 ppb to 2.81 ppb upon accounting for UGS-BVOCs
648 and UGS-LUCC. Given that the UGS are often located in densely populated urban regions, their
649 inclusion in air quality simulations is crucial for accurately modeling urban air quality.

- 650 3. The UGS-BVOC emissions have a significant impact on ozone concentrations, with increases ranging
651 from 1.0-1.4 ppb (+2.3-3.2%) in the city center regions. However, when considering the combined
652 UGS-LUCC and UGS-BVOC effects, the impact on MDA8 O₃ concentrations becomes remarkable,
653 with values ranging from 1.7-3.7 ppb (+3.8-8.5%) in the city center region. This indicates the
654 importance of considering both UGS-LUCC and UGS-BVOC impacts when discussing the influence
655 of UGS on air quality. Since UGS exhibits different effects in various ozone episodes, it is found that
656 the impact of UGS on ozone levels is related to specific meteorological conditions. In the episodes of
657 this study, the combined effects on MDA8 O₃ can reach up to 8.9 ppb in the city center region.

658
659 In this study, we used land use and land cover data integrated at 1 km and 10 m resolutions to define the urban
660 boundary and characterize the spatial distribution of UGS in Guangzhou. Additionally, we incorporate high-
661 resolution LAI data, obtained through machine learning, as input for the MEGAN model. Using the WRF-
662 CMAQ model, we quantify the effects of UGS-BVOC, UGS-LUCC, and their combined impacts on ozone
663 concentrations in Guangzhou. However, some uncertainties and limitations remain [in this study.](#)

664
665 First, the 10-m resolution land use and land cover data still cannot fully capture the spatial pattern of UGS in
666 Guangzhou. As shown in Figure S2, although UGS in Guangzhou is primarily composed of EBTs, most of
667 these EBTs are distributed along urban edges. This may result from distortions in the definition of urban extent,

668 such as misclassifying mixed urban-vegetation grids as urban grids, caused by the coarse resolution of the 1-
669 km land use and land cover data. The fuzzy definition of urban boundaries could lead to non-UGS areas being
670 misclassified as UGS, potentially resulting in an overestimation of UGS-BVOC emissions.

671
672 Second, due to resolution limitations, only larger patches of grassland, cropland, and woodland are recognized
673 as UGS, while smaller UGS vegetation, such as street trees, often goes undetected at a 10-m resolution. This
674 omission can lead to an underestimation of the UGS-BVOC emissions.

675
676 Third, the 10-m and 1-km resolution land use and land cover data, along with the growth forms and ecotype
677 data, use simplified categorizations for grids, which cannot fully capture the diversity of vegetation species
678 within UGS. Since different vegetation species have varying emission factors, this simplification introduces
679 some errors. Similarly, the oversimplified classification of land grids limits this study's ability to provide
680 specific planning strategies for UGS at the species level. Nevertheless, it can highlight the importance of
681 considering UGS-BVOC and UGS-LUCC in air pollution prevention and control policies.

682
683 Finally, Guangzhou, the study area, is a highly urbanized Chinese metropolis with a VOC-limited region
684 (Gong et al., 2018; Liu et al., 2018; Zhou Kai et al., 2011). As a result, even a relatively small amount of VOC
685 emissions, such as those from UGS-BVOC, can significantly impact ozone concentrations. Therefore,
686 policymakers in Guangzhou should prioritize addressing the role of UGS-BVOC emissions in air pollution
687 prevention and control. In other cities, particularly those with advanced urban development, high NO_x
688 emissions—often resulting from factors like high motor vehicle ownership—can lead to VOC-limited
689 conditions. In such areas, it is equally important to emphasize the role of UGS-BVOC emissions in ozone
690 pollution. In contrast, cities with lower NO_x emissions identified as NO_x-limited regions may experience
691 minimal impact from UGS-BVOC emissions on ozone concentrations.

692
693
694 This study on ozone pollution in Guangzhou provides key insights for other cities on integrating UGS with
695 air quality management. By including UGS-BVOC emissions and UGS-LUCC in the air quality model, the
696 study demonstrates improved accuracy in predicting surface ozone concentrations, which can aid urban
697 planners and environmental policymakers in refining their strategies to better address urban air pollution.
698 Moreover, these findings encourage cities to integrate urban forestry into their land use planning and air quality

699 frameworks, promoting environmental sustainability amid rapid urbanization.

700 **Data availability**

701 The WRF (Weather Research and Forecasting Model) code can be obtained from the official repository at
702 <https://github.com/wrf-model/WRF>. The CMAQ (Community Multiscale Air Quality Model) code is
703 accessible at <https://github.com/USEPA/CMAQ>. Model output data used for analysis and plotting, and the
704 code used for simulations can be made available upon request (Haofan Wang, wanghf58@mail2.sysu.edu.cn).

705 **Author contributions**

706 HFW conceived the study, carried out the model simulations, and drafted the manuscript. YJL completed the
707 data visualization. YML conceived and supervised this study, and reviewed and edited the paper. XL and YZ
708 provided useful comments on the paper. QF supervised and funded the study. CS provided the meteorological
709 data for model evaluation. SCL, YZ, TZ, and DLY provided the observation data for the evaluation of isoprene
710 simulation.

711 **Competing interests**

712 The contact author has declared that neither they nor their co-authors have any competing interests.

713 **Acknowledgment**

714 The authors would like to thank the MEIC team from Tsinghua University for providing the anthropogenic
715 emissions for this study. Meanwhile, we also thank Tianhe-2 for providing the computer resources.

716 **Financial support**

717 This work is jointly funded by the innovation Group Project of Southern Marine Science and Engineering
718 Guangdong Laboratory (Zhuhai) (316323005), Guangdong Basic and Applied Basic Research Foundation
719 (2020B0301030004, 2023A1515110103, 2023A1515010162), National Natural Science Foundation of China

(42105097, 42075181, 42375182), Guangdong Science and Technology Planning Project (2019B121201002), and Science and Technology Planning Project of Guangzhou (2023A04J1544).

Reference

- Allen, M.R., Ingram, W.J., 2002. Constraints on future changes in climate and the hydrologic cycle. *Nature* 419, 224–232. <https://doi.org/10.1038/nature01092>
- Arghavani, S., Malakooti, H., Bidokhti, A.A., 2019. Numerical evaluation of urban green space scenarios effects on gaseous air pollutants in Tehran Metropolis based on WRF-Chem model. *Atmos. Environ.* 214, 116832. <https://doi.org/10.1016/j.atmosenv.2019.116832>
- Burnett, R., Chen, H., Szyszkowicz, M., Fann, N., Hubbell, B., Pope, C.A., Apte, J.S., Brauer, M., Cohen, A., Weichenthal, S., Coggins, J., Di, Q., Brunekreef, B., Frostad, J., Lim, S.S., Kan, H., Walker, K.D., Thurston, G.D., Hayes, R.B., Lim, C.C., Turner, M.C., Jerrett, M., Krewski, D., Gapstur, S.M., Diver, W.R., Ostro, B., Goldberg, D., Crouse, D.L., Martin, R.V., Peters, P., Pinault, L., Tjepkema, M., van Donkelaar, A., Villeneuve, P.J., Miller, A.B., Yin, P., Zhou, M., Wang, L., Janssen, N.A.H., Marra, M., Atkinson, R.W., Tsang, H., Quoc Thach, T., Cannon, J.B., Allen, R.T., Hart, J.E., Laden, F., Cesaroni, G., Forastiere, F., Weinmayr, G., Jaensch, A., Nagel, G., Concin, H., Spadaro, J.V., Burnett, R., Chen, H., Szyszkowicz, M., Fann, N., Hubbell, B., Pope, C.A., Apte, J.S., Brauer, M., Cohen, A., Weichenthal, S., Coggins, J., Di, Q., Brunekreef, B., Frostad, J., Lim, S.S., Kan, H., Walker, K.D., Thurston, G.D., Hayes, R.B., Lim, C.C., Turner, M.C., Jerrett, M., Krewski, D., Gapstur, S.M., Diver, W.R., Ostro, B., Goldberg, D., Crouse, D.L., Martin, R.V., Peters, P., Pinault, L., Tjepkema, M., van Donkelaar, A., Villeneuve, P.J., Miller, A.B., Yin, P., Zhou, M., Wang, L., Janssen, N.A.H., Marra, M., Atkinson, R.W., Tsang, H., Quoc Thach, T., Cannon, J.B., Allen, R.T., Hart, J.E., Laden, F., Cesaroni, G., Forastiere, F., Weinmayr, G., Jaensch, A., Nagel, G., Concin, H., Spadaro, J.V., Burnett, R., Chen, H., Szyszkowicz, M., Fann, N., Hubbell, B., Pope, C.A., Apte, J.S., Brauer, M., Cohen, A., Weichenthal, S., Coggins, J., Di, Q., Brunekreef, B., Frostad, J., Lim, S.S., Kan, H., Walker, K.D., Thurston, G.D., Hayes, R.B., Lim, C.C., Turner, M.C., Jerrett, M., Krewski, D., Gapstur, S.M., Diver, W.R., Ostro, B., Goldberg, D., Crouse, D.L., Martin, R.V., Peters, P., Pinault, L., Tjepkema, M., van Donkelaar, A., Villeneuve, P.J., Miller, A.B., Yin, P., Zhou, M., Wang, L., Janssen, N.A.H., Marra, M., Atkinson, R.W., Tsang, H., Quoc Thach, T., Cannon, J.B., Allen, R.T., Hart, J.E., Laden, F., Cesaroni, G., Forastiere, F., Weinmayr, G., Jaensch, A., Nagel, G., Concin, H., Spadaro, J.V., 2018. Global estimates of mortality associated with long-term exposure to outdoor fine particulate matter. *Proc. Natl. Acad. Sci.* 115, 9592–9597. <https://doi.org/10.1073/pnas.1803222115>
- Cao, J., Situ, S., Hao, Y., Xie, S., Li, L., 2022. Enhanced summertime ozone and SOA from biogenic volatile organic compound (BVOC) emissions due to vegetation biomass variability during 1981–2018 in China. *Atmospheric Chem. Phys.* 22, 2351–2364. <https://doi.org/10.5194/acp-22-2351-2022>
- Chen, X., Wang, X., Wu, X., Guo, J., Zhou, Z., 2021. Influence of roadside vegetation barriers on air quality inside urban street canyons. *Urban For. Urban Green.* 63, 127219. <https://doi.org/10.1016/j.ufug.2021.127219>
- Chowdhury, S., Pozzer, A., Haines, A., Klingmueller, K., Muenzel, T., Paasonen, P., Sharma, A., Venkataraman, C., Lelieveld, J., 2022. Global health burden of ambient PM_{2.5} and the contribution of anthropogenic black carbon and organic aerosols. *Environ. Int.* 159, 107020.
- Cohen, A.J., Brauer, M., Burnett, R., Anderson, H.R., Frostad, J., Estep, K., Balakrishnan, K., Brunekreef, B., Dandona, L., Dandona, R., Feigin, V., Freedman, G., Hubbell, B., Jobling, A., Kan, H., Knibbs, L., Liu,

- 762 Y., Martin, R., Morawska, L., Pope, C.A., Shin, H., Straif, K., Shaddick, G., Thomas, M., van Dingenen,
763 R., van Donkelaar, A., Vos, T., Murray, C.J.L., Forouzanfar, M.H., 2017. Estimates and 25-year trends
764 of the global burden of disease attributable to ambient air pollution: an analysis of data from the Global
765 Burden of Diseases Study 2015. *The Lancet* 389, 1907–1918. [https://doi.org/10.1016/S0140-6736\(17\)30505-6](https://doi.org/10.1016/S0140-6736(17)30505-6)
- 767 Dunlea, E.J., Herndon, S.C., Nelson, D.D., Volkamer, R.M., San Martini, F., Sheehy, P.M., Zahniser, M.S.,
768 Shorter, J.H., Wormhoudt, J.C., Lamb, B.K., Allwine, E.J., Gaffney, J.S., Marley, N.A., Grutter, M.,
769 Marquez, C., Blanco, S., Cardenas, B., Retama, A., Ramos Villegas, C.R., Kolb, C.E., Molina, L.T.,
770 Molina, M.J., 2007. Evaluation of nitrogen dioxide chemiluminescence monitors in a polluted urban
771 environment. *Atmospheric Chem. Phys.* 7, 2691–2704. <https://doi.org/10.5194/acp-7-2691-2007>
- 772 Emery, C., Liu, Z., Russell, A.G., Odman, M.T., Yarwood, G., Kumar, N., 2017. Recommendations on
773 statistics and benchmarks to assess photochemical model performance. *J. Air Waste Manag. Assoc.* 67,
774 582–598. <https://doi.org/10.1080/10962247.2016.1265027>
- 775 Friedl, M., Sulla-Menashe, D., 2019. MCD12Q1 MODIS/Terra+Aqua Land Cover Type Yearly L3 Global
776 500m SIN Grid V006. <https://doi.org/10.5067/MODIS/MCD12Q1.006>
- 777 Fuhrer, J., Skärby, L., Ashmore, M.R., 1997. Critical levels for ozone effects on vegetation in Europe. *Environ.*
778 *Pollut.* 97, 91–106. [https://doi.org/10.1016/S0269-7491\(97\)00067-5](https://doi.org/10.1016/S0269-7491(97)00067-5)
- 779 Gong, J., Hu, Z., Chen, W., Liu, Y., Wang, J., Liu, Z., Doherty, R.M., Wild, O., Hollaway, M., O'Connor,
780 F.M., 2018. Urban expansion dynamics and modes in metropolitan Guangzhou, China. *Atmospheric*
781 *Chem. Phys.* 72, 100–109. <https://doi.org/10.1016/j.landusepol.2017.12.025>
- 782 Guenther, A., Jiang, X., Shah, T., Huang, L., Kemball-Cook, S., Yarwood, G., 2020a. Model of Emissions of
783 Gases and Aerosol from Nature Version 3 (MEGAN3) for Estimating Biogenic Emissions, in: Mensink,
784 C., Gong, W., Hakami, A. (Eds.), *Air Pollution Modeling and Its Application XXVI*, Springer
785 *Proceedings in Complexity*. Springer International Publishing, Cham, pp. 187–192.
786 https://doi.org/10.1007/978-3-030-22055-6_29
- 787 Guenther, A., Jiang, X., Shah, T., Huang, L., Kemball-Cook, S., Yarwood, G., 2020b. Model of Emissions of
788 Gases and Aerosol from Nature Version 3 (MEGAN3) for Estimating Biogenic Emissions, in: Mensink,
789 C., Gong, W., Hakami, A. (Eds.), *Air Pollution Modeling and Its Application XXVI*, Springer
790 *Proceedings in Complexity*. Springer International Publishing, Cham, pp. 187–192.
791 https://doi.org/10.1007/978-3-030-22055-6_29
- 792 Guenther, A.B., Jiang, X., Heald, C.L., Sakulyanontvittaya, T., Duhl, T., Emmons, L.K., Wang, X., 2012a.
793 The Model of Emissions of Gases and Aerosols from Nature version 2.1 (MEGAN2.1): an extended and
794 updated framework for modeling biogenic emissions. *Geosci. Model Dev.* 5, 1471–1492.
795 <https://doi.org/10.5194/gmd-5-1471-2012>
- 796 Guenther, A.B., Jiang, X., Heald, C.L., Sakulyanontvittaya, T., Duhl, T., Emmons, L.K., Wang, X., 2012b.
797 The Model of Emissions of Gases and Aerosols from Nature version 2.1 (MEGAN2.1): an extended and
798 updated framework for modeling biogenic emissions. *Geosci. Model Dev.* 5, 1471–1492.
799 <https://doi.org/10.5194/gmd-5-1471-2012>
- 800 He, C.Q., Zou, Y., Lv, S.J., Flores, R.M., Yan, X.L., Deng, T., Deng, X.J., 2024. The importance of
801 photochemical loss to source analysis and ozone formation potential: Implications from in-situ
802 observations of volatile organic compounds (VOCs) in Guangzhou, China. *Atmos. Environ.* 320, 120320.
803 <https://doi.org/10.1016/j.atmosenv.2023.120320>
- 804 Jin, S., Guo, J., Wheeler, S., Kan, L., Che, S., Fu, X., Liu, J., Ban-Weiss, G.A., Zhang, J., Huang, X., Ouyang,
805 B., Popoola, O., Tao, S., Tiwari, A., Kumar, P., Xing, Y., Brimblecombe, P., 2017. Effects of canyon
806 geometry on the distribution of traffic-related air pollution in a large urban area: Implications of a multi-
807 canyon air pollution dispersion model. *Atmos. Environ.* 165, 111–121.

808 <https://doi.org/10.1016/j.atmosenv.2017.06.031>

809 Jin, S., Guo, J., Wheeler, S., Kan, L., Che, S., Fu, X., Liu, J., Ban-Weiss, G.A., Zhang, J., Huang, X., Ouyang,
810 B., Popoola, O., Tao, S., Tiwari, A., Kumar, P., Xing, Y., Brimblecombe, P., 2014. Evaluation of impacts
811 of trees on PM_{2.5} dispersion in urban streets. *Atmos. Environ.* 99, 277–287.
812 <https://doi.org/10.1016/j.atmosenv.2014.10.002>

813 Le Page, Y., Morton, D., Bond-Lamberty, B., Pereira, J.M.C., Hurtt, G., 2015. HESFIRE: a global fire model
814 to explore the role of anthropogenic and weather drivers. *Biogeosciences* 12, 887–903.
815 <https://doi.org/10.5194/bg-12-887-2015>

816 Lelieveld, J., Klingmüller, K., Pozzer, A., Burnett, R.T., Haines, A., Ramanathan, V., 2019. Effects of fossil
817 fuel and total anthropogenic emission removal on public health and climate. *Proc. Natl. Acad. Sci.* 116,
818 7192–7197. <https://doi.org/10.1073/pnas.1819989116>

819 Lelieveld, J., Pozzer, A., Pöschl, U., Fnais, M., Haines, A., Münzel, T., 2020. Loss of life expectancy from air
820 pollution compared to other risk factors: a worldwide perspective. *Cardiovasc. Res.* 116, 1910–1917.

821 Li, S., Lu, X., Wang, H., 2024. Anthropogenic emission controls reduce summertime ozone-temperature
822 sensitivity in the United States. <https://doi.org/10.5194/egusphere-2024-1889>

823 Liu, Z., Doherty, R., Wild, O., Hollaway, M., O’Connor, F., 2018. Contrasting chemical environments in
824 summertime for atmospheric ozone across major Chinese industrial regions: the effectiveness of emission
825 control strategies. *Atmospheric Chem. Phys.* 21, 10689–10706. <https://doi.org/10.5194/acp-21-10689-2021>

826

827 Lohmann, U., Rotstajn, L., Storelvmo, T., Jones, A., Menon, S., Quaas, J., Ekman, A.M.L., Koch, D., Ruedy,
828 R., 2010. Total aerosol effect: radiative forcing or radiative flux perturbation? *Atmospheric Chem. Phys.*
829 10, 3235–3246. <https://doi.org/10.5194/acp-10-3235-2010>

830 Lombardozzi, D.L., Bonan, G.B., Smith, N.G., Dukes, J.S., Fisher, R.A., 2015. Temperature acclimation of
831 photosynthesis and respiration: A key uncertainty in the carbon cycle-climate feedback. *Geophys. Res.*
832 *Lett.* 42, 8624–8631. <https://doi.org/10.1002/2015GL065934>

833 Lu, X., Zhang, L., Wang, X., Gao, M., Li, K., Zhang, Yuzhong, Yue, X., Zhang, Yuanhang, 2020. Rapid
834 Increases in Warm-Season Surface Ozone and Resulting Health Impact in China Since 2013. *Environ.*
835 *Sci. Technol. Lett.* 7, 240–247. <https://doi.org/10.1021/acs.estlett.0c00171>

836 Luecken, D.J., Yarwood, G., Hutzell, W.T., 2019. Multipollutant modeling of ozone, reactive nitrogen and
837 HAPs across the continental US with CMAQ-CB6. *Atmos. Environ.* 201, 62–72.
838 <https://doi.org/10.1016/j.atmosenv.2018.11.060>

839 Ma, H., Liang, S., 2022. Development of the GLASS 250-m leaf area index product (version 6) from MODIS
840 data using the bidirectional LSTM deep learning model. *Remote Sens. Environ.* 273, 112985.
841 <https://doi.org/10.1016/j.rse.2022.112985>

842 Ma, M., Gao, Y., Ding, A., Su, H., Liao, H., Wang, S., Wang, X., Zhao, B., Zhang, S., Fu, P., Guenther, A.B.,
843 Wang, M., Li, S., Chu, B., Yao, X., Gao, H., 2022. Development and Assessment of a High-Resolution
844 Biogenic Emission Inventory from Urban Green Spaces in China. *Environ. Sci. Technol.* 56, 175–184.
845 <https://doi.org/10.1021/acs.est.1c06170>

846 Ma, M., Gao, Y., Wang, Y., Zhang, S., Leung, L.R., Liu, C., Wang, S., Zhao, B., Chang, X., Su, H., Zhang,
847 T., Sheng, L., Yao, X., Gao, H., 2019. Substantial ozone enhancement over the North China Plain from
848 increased biogenic emissions due to heat waves and land cover in summer 2017. *Atmospheric Chem.*
849 *Phys.* 19, 12195–12207. <https://doi.org/10.5194/acp-19-12195-2019>

850 Masson-Delmotte, V., Zhai, P., Pirani, A., Connors, S.L., Péan, C., Berger, S., Caud, N., Chen, Y., Goldfarb,
851 L., Gomis, M., others, 2021. Climate change 2021: the physical science basis. *Contrib. Work. Group*
852 *Sixth Assess. Rep. Intergov. Panel Clim. Change* 2.

853 Meng, Y., Song, J., Zeng, L., Zhang, Y., Zhao, Y., Liu, X., Guo, H., Zhong, L., Ou, Y., Zhou, Y., Zhang, T.,

854 Yue, D., Lai, S., 2022. Ambient volatile organic compounds at a receptor site in the Pearl River Delta
855 region: Variations, source apportionment and effects on ozone formation. *J. Environ. Sci.* 111, 104–117.
856 <https://doi.org/10.1016/j.jes.2021.02.024>

857 Myneni, R., Knyazikhin, Y., Park, T., 2015. MOD15A2H MODIS/Terra leaf area Index/FPAR 8-Day L4
858 global 500m SIN grid V006. NASA EOSDIS Land Process. DAAC.

859 National Centers for Environmental Prediction, National Weather Service, NOAA, U.S. Department of
860 Commerce, 2000. NCEP FNL Operational Model Global Tropospheric Analyses, continuing from July
861 1999.

862 Pye, H.O.T., Murphy, B.N., Xu, L., Ng, N.L., Carlton, A.G., Guo, H., Weber, R., Vasilakos, P., Appel, K.W.,
863 Budisulistiorini, S.H., Surratt, J.D., Nenes, A., Hu, W., Jimenez, J.L., Isaacman-VanWertz, G., Misztal,
864 P.K., Goldstein, A.H., 2017. On the implications of aerosol liquid water and phase separation for organic
865 aerosol mass. *Atmospheric Chem. Phys.* 17, 343–369. <https://doi.org/10.5194/acp-17-343-2017>

866 Qiu, J., Fang, C., Tian, N., Wang, H., Wang, J., 2023. Impacts of land use and land cover changes on local
867 meteorology and PM_{2.5} concentrations in Changchun, Northeast China. *Atmospheric Res.* 289, 106759.
868 <https://doi.org/10.1016/j.atmosres.2023.106759>

869 Ramanathan, V., Crutzen, P.J., Kiehl, J.T., Rosenfeld, D., Ramanathan, V., Crutzen, P.J., Kiehl, J.T.,
870 Rosenfeld, D., Ramanathan, V., Crutzen, P.J., Kiehl, J.T., Rosenfeld, D., 2001. Aerosols, Climate, and
871 the Hydrological Cycle. *Science* 294, 2119–2124. <https://doi.org/10.1126/science.1064034>

872 Salamanca, F., Martilli, A., Tewari, M., Chen, F., 2011. A Study of the Urban Boundary Layer Using Different
873 Urban Parameterizations and High-Resolution Urban Canopy Parameters with WRF. *J. Appl. Meteorol.*
874 *Climatol.* 50, 1107–1128. <https://doi.org/10.1175/2010JAMC2538.1>

875 Schlaerth, H.L., Silva, S.J., Li, Y., 2023. Characterizing Ozone Sensitivity to Urban Greening in Los Angeles
876 Under Current Day and Future Anthropogenic Emissions Scenarios. *J. Geophys. Res. Atmospheres* 128,
877 e2023JD039199. <https://doi.org/10.1029/2023JD039199>

878 Seinfeld, J.H., Pandis, S.N., Noone, K., 1998. *Atmospheric Chemistry and Physics: From Air Pollution to*
879 *Climate Change*. *Phys. Today* 51, 88–90. <https://doi.org/10.1063/1.882420>

880 Shan, D., Du, Z., Zhang, T., Zhang, X., Cao, G., Liu, Z., Yao, Z., Tang, K., Liang, S., 2023. Variations, sources,
881 and effects on ozone formation of VOCs during ozone episodes in 13 cities in China. *Front. Environ. Sci.*
882 10, 1084592. <https://doi.org/10.3389/fenvs.2022.1084592>

883 Shindell, D., Kuylensstierna, J.C.I., Vignati, E., van Dingenen, R., Amann, M., Klimont, Z., Anenberg, S.C.,
884 Muller, N., Janssens-Maenhout, G., Raes, F., Schwartz, J., Faluvegi, G., Pozzoli, L., Kupiainen, K.,
885 Höglund-Isaksson, L., Emberson, L., Streets, D., Ramanathan, V., Hicks, K., Oanh, N.T.K., Milly, G.,
886 Williams, M., Demkine, V., Fowler, D., Shindell, D., Kuylensstierna, J.C.I., Vignati, E., van Dingenen,
887 R., Amann, M., Klimont, Z., Anenberg, S.C., Muller, N., Janssens-Maenhout, G., Raes, F., Schwartz, J.,
888 Faluvegi, G., Pozzoli, L., Kupiainen, K., Höglund-Isaksson, L., Emberson, L., Streets, D., Ramanathan,
889 V., Hicks, K., Oanh, N.T.K., Milly, G., Williams, M., Demkine, V., Fowler, D., Shindell, D.,
890 Kuylensstierna, J.C.I., Vignati, E., van Dingenen, R., Amann, M., Klimont, Z., Anenberg, S.C., Muller,
891 N., Janssens-Maenhout, G., Raes, F., Schwartz, J., Faluvegi, G., Pozzoli, L., Kupiainen, K., Höglund-
892 Isaksson, L., Emberson, L., Streets, D., Ramanathan, V., Hicks, K., Oanh, N.T.K., Milly, G., Williams,
893 M., Demkine, V., Fowler, D., 2012. Simultaneously Mitigating Near-Term Climate Change and
894 Improving Human Health and Food Security. *Science* 335, 183–189.
895 <https://doi.org/10.1126/science.1210026>

896 Soleimani, E., Wang, Y., Li, W., Liu, X., Griggs, T., Flynn, J., Walter, P.J., Estes, M.J., 2023. Understanding
897 ozone episodes during the TRACER-AQ campaign in Houston, Texas: The role of transport and ozone
898 production sensitivity to precursors. *Sci. Total Environ.* 900, 165881.
899 <https://doi.org/10.1016/j.scitotenv.2023.165881>

- 900 Solomon, S., 2007. Climate change 2007-the physical science basis: Working group I contribution to the
901 fourth assessment report of the IPCC. Cambridge university press.
- 902 Tiwari, A., Kumar, P., 2020. Integrated dispersion-deposition modelling for air pollutant reduction via green
903 infrastructure at an urban scale. *Sci. Total Environ.* 723, 138078.
904 <https://doi.org/10.1016/j.scitotenv.2020.138078>
- 905 Tomson, M., Kumar, P., Barwise, Y., Perez, P., Forehead, H., French, K., Morawska, L., Watts, J.F., 2021.
906 Green infrastructure for air quality improvement in street canyons. *Environ. Int.* 146, 106288.
907 <https://doi.org/10.1016/j.envint.2020.106288>
- 908 Wang, H., Liu, Z., Wu, K., Qiu, J., Zhang, Y., Ye, B., He, M., 2022. Impact of Urbanization on Meteorology
909 and Air Quality in Chengdu, a Basin City of Southwestern China. *Front. Ecol. Evol.* 10, 845801.
910 <https://doi.org/10.3389/fevo.2022.845801>
- 911 Wang, H., Liu, Z., Zhang, Y., Yu, Z., Chen, C., 2021. Impact of different urban canopy models on air quality
912 simulation in Chengdu, southwestern China. *Atmos. Environ.* 267, 118775.
913 <https://doi.org/10.1016/j.atmosenv.2021.118775>
- 914 Wang, N., Lyu, X., Deng, X., Huang, X., Jiang, F., Ding, A., 2019a. Role of vegetation in deposition and
915 dispersion of air pollution in urban parks. *Atmos. Environ.* 201, 73–83.
916 <https://doi.org/10.1016/j.atmosenv.2018.12.027>
- 917 Wang, N., Lyu, X., Deng, X., Huang, X., Jiang, F., Ding, A., 2019b. Aggravating O₃ pollution due to NO_x
918 emission control in eastern China. *Sci. Total Environ.* 677, 732–744.
919 <https://doi.org/10.1016/j.scitotenv.2019.04.388>
- 920 Wang, P., Chen, Y., Hu, J., Zhang, H., Ying, Q., 2019. Attribution of Tropospheric Ozone to NO_x and VOC
921 Emissions: Considering Ozone Formation in the Transition Regime. *Environ. Sci. Technol.* 53, 1404–
922 1412. <https://doi.org/10.1021/acs.est.8b05981>
- 923 WHO, 2021. WHO global air quality guidelines: particulate matter (PM_{2.5} and PM₁₀), ozone, nitrogen
924 dioxide, sulfur dioxide and carbon monoxide. World Health Organization.
- 925 Wu, K., Yang, X., Chen, D., Gu, S., Lu, Y., Jiang, Q., Wang, K., Ou, Y., Qian, Y., Shao, P., Lu, S., 2020.
926 Estimation of biogenic VOC emissions and their corresponding impact on ozone and secondary organic
927 aerosol formation in China. *Atmospheric Res.* 231, 104656.
928 <https://doi.org/10.1016/j.atmosres.2019.104656>
- 929 Yang, H., Chen, T., Lin, Y., Buccolieri, R., Mattsson, M., Zhang, M., Hang, J., Wang, Q., 2020. Integrated
930 impacts of tree planting and street aspect ratios on CO dispersion and personal exposure in full-scale
931 street canyons. *Build. Environ.* 169, 106529. <https://doi.org/10.1016/j.buildenv.2019.106529>
- 932 Yao, Z., Huang, G., 2023. Effects of Land Use Changes Across Different Urbanization Periods on Summer
933 Rainfall in the Pearl River Delta Core Area. *Int. J. Disaster Risk Sci.* 14, 458–474.
934 <https://doi.org/10.1007/s13753-023-00497-8>
- 935 Yim, S.H.L., Wang, M., Gu, Y., Yang, Y., Dong, G., Li, Q., 2019. Effect of Urbanization on Ozone and
936 Resultant Health Effects in the Pearl River Delta Region of China. *J. Geophys. Res. Atmospheres* 124,
937 11568–11579. <https://doi.org/10.1029/2019JD030562>
- 938 Zhang, Y., Cao, F., 2015. Fine particulate matter (PM_{2.5}) in China at a city level, *Sci. Rep.*, 5, 14884.
- 939 Zheng, J., Shao, M., Che, W., Zhang, L., Zhong, L., Zhang, Y., Streets, D., 2009. Speciated VOC Emission
940 Inventory and Spatial Patterns of Ozone Formation Potential in the Pearl River Delta, China. *Environ.*
941 *Sci. Technol.* 43, 8580–8586. <https://doi.org/10.1021/es901688e>
- 942 Zhou, D., Zhao, S., Zhang, L., Sun, G., Liu, Y., 2015. The footprint of urban heat island effect in China. *Sci.*
943 *Rep.* 5, 11160.
- 944 Zhou Kai, Zhang Wen-jie, Wang Zhi-fang, Cao Wei, Peng Shao-lin, 2011. The influence of urbanization on
945 atmospheric environmental quality in Guangzhou, China. 2011 Int. Conf. Electr. Technol. Civ. Eng.

946
947

ICETCE 3667–3670. <https://doi.org/10.1109/ICETCE.2011.5776281>